



## Electrochemical Kinetic Studies of Li-Ion in O2-Structured $\text{Li}_{2/3}(\text{Ni}_{1/3}\text{Mn}_{2/3})\text{O}_2$ and $\text{Li}_{(2/3)+x}(\text{Ni}_{1/3}\text{Mn}_{2/3})\text{O}_2$ by EIS and GITT

K. M. Shaju, G. V. Subba Rao, and B. V. R. Chowdari<sup>z</sup>

Department of Physics, National University of Singapore, Singapore 119260

The kinetics of Li-ion intercalation into O2 structure layered nickel-manganese oxides,  $\text{Li}_{2/3}(\text{Ni}_{1/3}\text{Mn}_{2/3})\text{O}_2$  [O2 (Li)] and  $\text{Li}_{(2/3)+x}(\text{Ni}_{1/3}\text{Mn}_{2/3})\text{O}_2$ ,  $x = 1/3$  [O2 (Li + x)] were determined by electrochemical impedance spectroscopy (EIS) and galvanostatic intermittent titration technique (GITT) in conjunction with other electrochemical techniques. Modeling the EIS data with equivalent circuit approach enabled the determination of charge transfer, bulk, and surface film resistances. The formation and nature of surface film is shown to be the signature for the cell performance which in turn affects the kinetics of electrode processes. The improved cycling performance of O2 (Li + x) is shown to be due to the better electrode kinetics and the formation of stable surface film. The Li-ion diffusion coefficient ( $D_{\text{Li}}$ ) was determined at different cell potentials by GITT on O2 (Li) and O2 (Li + x) and analyzing the Warburg region of the impedance plots of O2 (Li + x). The  $D_{\text{Li}}$  values are in the range  $1.0 \times 10^{-11}$  to  $10^{-10}$  cm<sup>2</sup>/s for both the compounds in the entire composition (voltage) range. The  $D_{\text{Li}}$  (GITT) values are lower by a factor of two as compared to those obtained from EIS in the entire voltage range for O2 (Li + x). The irreversible phase change from the T2 to O2 structure observed during the first charging in these compounds, is reflected as minima in the  $D_{\text{Li}}$  vs. voltage plots in the vicinity of the cyclic voltammetric peaks.

© 2002 The Electrochemical Society. [DOI: 10.1149/1.1521754] All rights reserved.

Manuscript submitted February 15, 2002; revised manuscript received June 14, 2002. Available electronically November 15, 2002.

Recently, layered nickel manganese oxide, O2- $\text{Li}_{2/3}(\text{Ni}_{1/3}\text{Mn}_{2/3})\text{O}_2$  has been synthesized and studied by Dahn and his co-workers<sup>1-4</sup> as the cathode material for Li-ion batteries. The stable cycling performance observed for this compound, as compared to  $\text{LiMnO}_2$  is due to the fact that the oxygen stacking sequence in the O2-phase compounds necessitates breaking and rearrangement of M-O (M = Ni, Mn) bonds to convert it to the spinel structure, whereas for the O3- $\text{LiMnO}_2$  a minor cationic rearrangement can lead to the spinel structure.<sup>1,2,5-7</sup> O3 and O2 structure implies an octahedral oxygen coordination for Li ions and the unit cell contains 3 and 2  $\text{MO}_2$  layers, respectively. The O2 compound is obtained by ion exchanging the P2-phase  $\text{Na}_{2/3}(\text{Ni}_{1/3}\text{Mn}_{2/3})\text{O}_2$  which can be prepared by high temperature solid-state reaction (P2 implies trigonal prismatic oxygen coordination for Li ions and the unit cell contains 2  $\text{MO}_2$  layers). The P2 to O2 structure conversion involves only minor sliding of the  $\text{MO}_2$  sheets with respect to one another in the layer structure and occurs during the ion exchange process. Detailed *in situ* XRD studies by Paulsen *et al.*<sup>1-3</sup> have shown that the P2 structure converts first to the T2 structure (distorted tetrahedral oxygen coordination of Li and superstructure-ordering of Ni and Mn ions in the  $\text{MO}_2$  sheets) during the Na to Li ion exchange. After the first cycle of electrochemical charge/discharge, the T2 to O2 conversion occurs, possibly with some stacking faults. Since the T2 and O2 structures are closely related, to a first approximation, the as-prepared  $\text{Li}_{2/3}(\text{Ni}_{1/3}\text{Mn}_{2/3})\text{O}_2$  can be indexed as O2 phase. O2- $\text{Li}_{2/3}(\text{Ni}_{1/3}\text{Mn}_{2/3})\text{O}_2$  as the positive (cathode) electrode was shown to give a reversible capacity of 180 mAh/g between 2.5 and 4.6 V vs. Li and good capacity retention during cycling at low C rates at 30 and 55°C.<sup>1-4,8,9</sup> However, the first extraction (charge) capacity of this material is found to be ~100 mAh/g and corresponds to only 1/3 mol of Li extraction. Charging the cell much above the usual voltage limit (up to 5.4 V vs. Li) did not show any indication of full extraction (2/3 mol) of Li from the compound.<sup>4</sup> This inability to extract all the Li from O2- $\text{Li}_{2/3}(\text{Ni}_{1/3}\text{Mn}_{2/3})\text{O}_2$  seems to be the inherent property of the compound, even though the reasons are not known. We have been able to incorporate extra lithium ( $x = 1/3$ ) to obtain O2- $\text{Li}_{(2/3)+x}(\text{Ni}_{1/3}\text{Mn}_{2/3})\text{O}_2$  using LiI as the reducing agent and showed that it gives a higher first extraction capacity together with highly

reversible and stable cycling performance as cathode vs. Li anode at 25 and 50°C.<sup>8</sup> The performance of this compound as cathode in Li-ion cell with mesocarbon microbead graphite has also been demonstrated. Further, the performance of the extra lithium incorporated compound is shown to be superior to the as prepared O2-phase compound with respect to its reversible capacity, cycling performance, and high current rate charge/discharge capability.<sup>8</sup>

Understanding of the kinetic parameters which control the performance and the processes which are responsible for the stabilization or failure of intercalation electrodes are crucial for their optimization in Li-ion batteries. The factors which control the rate of Li intercalation/deintercalation in layered intercalation compounds and the performance wherein depend on the bulk properties like diffusion of Li within the compound and its electronic conductivity as well as the kinetics of the electrochemical processes at the interface. The structural modification and phase transition (if any) of the electrode material at varying levels of intercalation (cell voltage and/or composition) and the morphological changes (particle to particle connectivity) brought about by repeated cycling also have substantial effects on the kinetics and hence the performance of the electrode. There are different opinions on the factors which affect and control the performance of the electrodes. The diffusion of Li ions within the intercalation compound was thought to be the process which controls the electrode kinetics. On the other hand it is assumed that the electronic charge transfer and the Li-ion adsorption at the electrode/electrolyte interface may be the rate determining step. Therefore, a quantitative study of lithiation/delithiation rates together with the determination of the diffusion coefficient of Li within the electrode would provide more insight into its performance. To this end, detailed study on the electrochemical performance together with various electroanalytical techniques proved to be helpful. The latter techniques which are commonly used are electrochemical impedance spectroscopy (EIS),<sup>10-28</sup> galvanostatic intermittent titration technique (GITT),<sup>29-34</sup> potentiostatic intermittent titration technique (PITT),<sup>35-37</sup> and slow scan cyclic voltammetry (SSCV).<sup>12,15,36</sup> Though the structural aspects and electrochemical performance of the O2-phase compounds,  $\text{Li}_{2/3}(\text{Ni}_{1/3}\text{Mn}_{2/3})\text{O}_2$  and  $\text{Li}_{2/3}(\text{Co}_{0.15}\text{Mn}_{0.85})\text{O}_2$ , have been elucidated,<sup>1-4,7-9</sup> there are no reports on the kinetic parameters which control the cell performance. Further, it would be informative to differentiate the factors which lead to an improved performance of the lithiated compound,  $\text{Li}_{1.0}(\text{Ni}_{1/3}\text{Mn}_{2/3})\text{O}_2$ .<sup>8</sup> The present report deals with EIS and GITT

<sup>z</sup> E-mail: phychowd@nus.edu.sg

studies on  $\text{Li}_{2/3}(\text{Ni}_{1/3}\text{Mn}_{2/3})\text{O}_2$  and  $\text{Li}_{1.0}(\text{Ni}_{1/3}\text{Mn}_{2/3})\text{O}_2$  to obtain the electrode kinetic parameters and to correlate them with the electrochemical performance.

### Experimental

The precursor compound,  $\text{Na}_{2/3}(\text{Ni}_{1/3}\text{Mn}_{2/3})\text{O}_2$  was synthesized by high temperature (900°C) solid-state reaction as described elsewhere.<sup>1,2,8,9</sup> Ion exchange for sodium to lithium was done using the melt of an eutectic mixture of  $\text{LiNO}_3$  and  $\text{LiCl}$  (88:12 mol %) at 280°C. After 2 h of soaking in the eutectic which contains seven times excess lithium, the melt was cooled, the product was dissolved in deionized water and the solution was filtered to recover the desired compound  $\text{Li}_{2/3}(\text{Ni}_{1/3}\text{Mn}_{2/3})\text{O}_2$ . The powder was dried at 100°C for 12 h in an air oven and used for characterization by X-ray diffraction (XRD) (Siemens D5005; Cu K $\alpha$  radiation) and chemical analysis. Incorporation of extra lithium ( $x$ ) was done during the ion exchange process using a fresh batch of the precursor. The ion exchange was allowed to proceed as described above for 1 h, after which solid powder of lithium iodide (mole ratio, compound:  $\text{LiI} = 1:0.6$ ) was added to the melt and the soaking was continued for two more hours. The product was then cooled to room temperature and the desired compound was recovered by the procedure described above and characterized.

Chemical analysis for Na, Li, Ni, and Mn in the compounds was done by inductively coupled plasma (ICP) spectroscopic analysis. The elemental concentration data were normalized to  $\text{Ni}_{0.33}$  assuming the total metal content to be 1.67 and 2.0 before and after  $\text{LiI}$  treatment of the compounds. The oxygen content was not determined and was assumed to be 2.0. For the electrochemical studies, the positive electrodes were fabricated as follows:<sup>7-9</sup> active material, super P carbon black as conducting additive, and Kynar 2801 as binder were mixed in 80:10:10 (wt %) ratio and made homogeneous slurry in *N*-methylpyrrolidinone. The viscous paste was then applied onto an etched aluminum (Al) foil (15  $\mu\text{m}$  thick and 25  $\text{cm}^2$  area) to form a thick layer (20–25  $\mu\text{m}$ ) by doctor blade technique. The film was then dried at 100°C in an air oven, smoothed by passing through a twin roller (stainless steel), and cut into circular strips of 16 mm diam. The strips were vacuum dried at 70°C for 12 h and kept in an argon filled glove box which maintains <1 ppm of  $\text{H}_2\text{O}$  and  $\text{O}_2$  (MBraun, Germany).

Coin cells (size 2016) were assembled in the glove box with 1 M  $\text{LiPF}_6$  in ethylene carbonate + diethyl carbonate (EC + DEC, 1:1 volume, Merck, Selectipur LP40) as the electrolyte and Celgard 2502 membrane as separator. Li metal foil (Kyokuto Metal Co., Japan) was cut into circular disks (16 mm diam) to cover the electrode area) and were used as anode. Charge/discharge cycling and cyclic voltammetry (CV) tests at 25°C were carried out with a potentiostat/galvanostat system (MacPile II, Bio-logic, France) and Bitrode multiple battery tester (model SCN, Bitrode, USA). For GITT measurement, the Bitrode battery tester was programmed to supply a constant current flux for a known time followed by open circuit stand for the specified time. The sequence was continued for the composition ( $x$  in  $\text{Li}_x\text{MO}_2$  or voltage) of interest and for the required number of charge/discharge cycles. EIS has been done using the Solartron impedance/gain-phase analyzer (SI 1260) coupled with a battery test unit (1470). The amplitude of the ac signal was kept at 5 mV and the frequency range of measurement was 0.35 MHz to 2 MHz. Impedance data acquisition and analysis were performed, respectively, by using the electrochemical impedance software ZPlot and Zview (version 2.2, Scribner Associates Inc.).

### Results and Discussion

**Composition and structure.**—The chemical composition obtained by ICP for the compounds  $\text{Na}_{2/3}(\text{Ni}_{1/3}\text{Mn}_{2/3})\text{O}_2$  [P2(Na)],  $\text{Li}_{2/3}(\text{Ni}_{1/3}\text{Mn}_{2/3})\text{O}_2$  [O2(Li)], and  $\text{Li}_{(2/3)+x}(\text{Ni}_{1/3}\text{Mn}_{2/3})\text{O}_2$  [O2(Li +  $x$ )], are  $\text{Na}_{0.61}(\text{Ni}_{0.33}\text{Mn}_{0.67})\text{O}_2$ ,  $\text{Li}_{0.67}\text{Na}_{0.005}(\text{Ni}_{0.33}\text{Mn}_{0.65})\text{O}_2$ ,

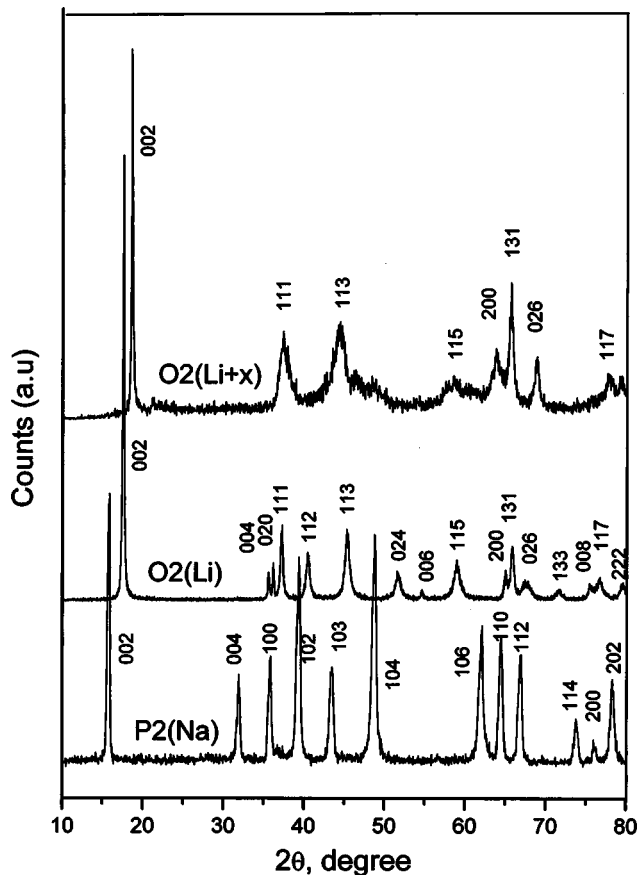


**Figure 1.** XRD patterns (Cu K $\alpha$  radiation) of  $\text{Na}_{2/3}(\text{Ni}_{1/3}\text{Mn}_{2/3})\text{O}_2$  [P2 (Na)],  $\text{Li}_{2/3}(\text{Ni}_{1/3}\text{Mn}_{2/3})\text{O}_2$  [O2 (Li)], and  $\text{Li}_{(2/3)+x}(\text{Ni}_{1/3}\text{Mn}_{2/3})\text{O}_2$  [O2 (Li +  $x$ )]. ( $hkl$ ) are shown.

and  $\text{Li}_{0.95}\text{Na}_{0.002}(\text{Ni}_{0.33}\text{Mn}_{0.67})\text{O}_2$ , respectively. The chemical analysis shows that the ion exchange for Na by Li is complete for both the compounds, O2 (Li) and O2 (Li +  $x$ ). Taking into account a  $\pm 5$ –8% uncertainty in determining the Na and Li content, and  $\pm 2$ –4% uncertainty in the analysis of Ni and Mn, the compounds show the expected stoichiometry. Further, it is evident that the incorporation of extra lithium ( $x \approx 1/3$ ) by the present lithiation technique is successful to give O2 (Li +  $x$ ).

The powder XRD patterns of P2 (Na), O2 (Li), and O2 (Li +  $x$ ) are shown in Fig. 1. The patterns of P2 (Na) and O2 (Li) compounds match well with those reported by Paulsen *et al.*<sup>1-3</sup> The hexagonal lattice parameters obtained for P2 (Na) after least squares fitting the ( $hkl$ ) and  $d$  values are  $a = 2.892 (\pm 0.001) \text{ \AA}$  and  $c = 11.23 (\pm 0.01) \text{ \AA}$ . The O2 (Li) is indexed as the T2 phase (orthorhombic, space group  $Cmca$ ) and the lattice parameters are  $a = 2.865 (\pm 0.001)$ ,  $b = 4.954 (\pm 0.002)$ , and  $c = 10.056 (\pm 0.004) \text{ \AA}$ . These values are in good agreement with the values reported by Paulsen *et al.*<sup>1-3</sup> The XRD pattern of the O2 (Li +  $x$ ) bears good resemblance to that of O2 (Li) and shows that the crystal system remains the same. The broadening of the XRD peaks for O2 (Li +  $x$ ) indicates that the  $\text{LiI}$  treatment leads to a reduction in its crystallite size. Further, a few lines which are present in O2 (Li) [*e.g.*, (004), (020), (112), and (024)] disappear in O2 (Li +  $x$ ). The reasons for this are not known at present but could be caused by the stacking faults in the lattice formed during the P2 to T2 (or O2) conversion. Similar XRD patterns were also observed by Paulsen and Dahn<sup>38</sup> for  $\text{Li}_{2/3}(\text{Li}_{1/6}\text{Mn}_{5/6})\text{O}_2$  and  $\text{Li}_{2/3}(\text{Co}_{0.15}\text{Mn}_{0.85})\text{O}_2$  and are shown to be due to the stacking faulted O2 structure. The orthorhombic lattice parameters obtained for O2 (Li +  $x$ ) are

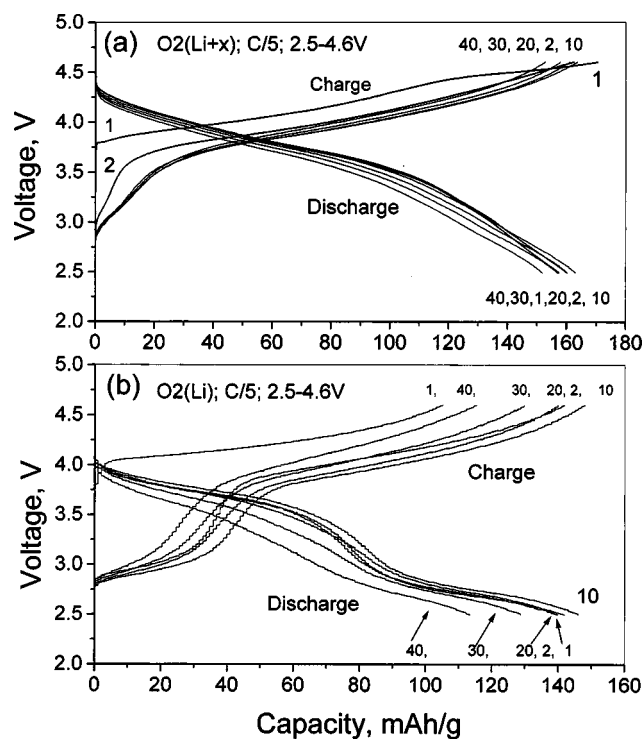
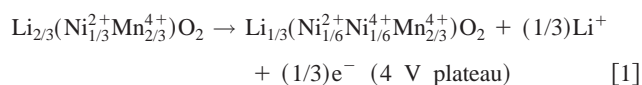
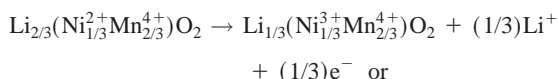


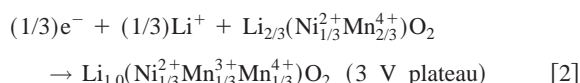
**Figure 2.** The voltage vs. cathodic capacity profile at C/5 rate for different charge/discharge cycles between 2.5 to 4.6 V (vs. Li) recorded at 25°C (a) O2(Li + x) and (b) O2(Li). Cycle numbers are indicated.

$a = 2.947 (\pm 0.004)$ ,  $b = 5.002 (\pm 0.007)$ , and  $c = 9.91 (\pm 0.01)$  Å. The larger values of  $a$  and  $b$  in O2(Li + x) compared to O2(Li) can be explained by the increased concentration of larger Mn<sup>3+</sup> ions in O2(Li + x) due to the reduction of 0.33 Mn<sup>4+</sup> ions by the LiI treatment. A significant reduction in the  $c$  lattice parameter as compared to the O2(Li) phase is observed for the O2(Li + x).<sup>8</sup> This is due to the fact that the 1/3 vacant sites in the O2(Li) are occupied by Li ions in the Li layer in O2(Li + x) thereby reducing the repulsive interaction between the oxide-ion layers.

**Electrochemical behavior of the O2(Li) and O2(Li + x) electrodes.**—Before analyzing the electroanalytical response and correlating it with the electrode kinetics, it is important to have the data on the electrochemical performance and kinetics of the electrodes together with its implications to the structural aspects. Particularly, it would be interesting to identify the change in Li-ion intercalation/deintercalation kinetics associated with the electrochemically assisted irreversible phase change (T2 to O2) observed for these compounds during their first deintercalation cycle.<sup>1-4,8,9</sup> The voltage vs. capacity profiles and the cycling performance at a C/5 rate for the O2(Li + x) and O2(Li) compounds as cathodes for different charge/discharge cycles between 2.5 to 4.6 V (vs. Li) are shown in Fig. 2. The O2(Li) shows only one extraction (Li deintercalation) plateau centered around 4 V with a capacity of 105 mAh/g. The low initial extraction capacity is due to the fact that only 1/3 mol of lithium can be extracted from the compound corresponding to the oxidation of 1/3 Ni<sup>2+</sup> to Ni<sup>3+</sup> or 1/6 Ni<sup>2+</sup> to Ni<sup>4+</sup> ions in the crystal lattice<sup>1,8</sup>



In principle, it should be possible to extract all the lithium from the cathode if the rest of the (1/6) Ni<sup>2+</sup> or (1/3) of Ni<sup>3+</sup> ions can be oxidized to Ni<sup>4+</sup> ions, similar to the case of O3-LiNi<sup>3+</sup>O<sub>2</sub> and Li(Ni,Co)<sup>3+</sup>O<sub>2</sub>.<sup>39,40</sup> The reason for the lower first extraction capacity in O2(Li) is still not clear and was discussed by Lu and Dahn.<sup>4</sup> The first-discharge profile of O2(Li) consists of two almost equally divided plateaus with a total capacity of 142 mAh/g. At C/10 rate we have observed a reversible capacity of 187 mAh/g which corresponds to ~2/3 mol of Li in the compound.<sup>8,9</sup> This higher discharge capacity, as compared to the initial charge capacity, is expected because in addition to the 1/3 mol Li insertion due to the reverse reaction as shown in Eq. 1, 1/3 mol of extra Li is added to the lattice with the simultaneous reduction of Mn<sup>4+</sup> as per the reaction



This is reproduced during the second charging process and subsequent charge/discharge cycles indicating that both Mn and Ni ions are participating in the redox processes. A reversible capacity of 180 mAh/g was reported by Dahn *et al.* at a low C rate (C/40) in the same voltage window.<sup>1-4</sup>

The first extraction capacity for O2(Li + x) is 171 mAh/g at C/5 rate. At C/10 rate it delivers 190 mAh/g which is almost equivalent to the removal of 2/3 mol of Li.<sup>8</sup> Comparing this value with the initial extraction capacity of the O2(Li) phase (105 mAh/g, ~1/3 mol Li) (Fig. 2b) confirms that the insertion of Li into the lattice has indeed taken place by our lithiation process using LiI. This led to a twofold increase in the first extraction capacity for the O2(Li + x) over O2(Li) and the chemical formula of O2(Li + x) can be written as Li<sub>1,0</sub>(Ni<sub>1/3</sub><sup>2+</sup>Mn<sub>1/3</sub><sup>3+</sup>Mn<sub>1/3</sub><sup>4+</sup>)O<sub>2</sub>.<sup>8</sup> This is in good agreement with the chemical analysis data on O2(Li + x). The oxidation processes taking place during the first charge in O2(Li + x) can be written as reverse processes of Eq. 2 and 1, respectively. The first discharge capacity is 158 mAh/g at C/5 rate. The performance of the electrode materials, O2(Li) and O2(Li + x) on repeated charge/discharge cycling is compared in Fig. 2. It can be seen that the capacity fade for the O2(Li + x) is minimal over 40 charge/discharge cycles. However, in the same voltage window and current rate, the capacity fade for O2(Li) after the 20th cycle is very prominent. It is also known that the rate capability of O2(Li + x) is much better than the cell with O2(Li) at 25 and 50°C.<sup>8</sup> Qualitative difference in the voltage vs. capacity curves of O2(Li + x) and O2(Li) can be clearly seen from Fig. 2a and b: a twofold increase in the first extraction capacity is observed for the O2(Li + x) over O2(Li) and a smooth capacity vs. voltage profile is observed for the O2(Li + x) as compared to a nearly 1 V drop in voltage for the O2(Li) in the 3.0-3.5 V (vs. Li) region. Further, an irreversible plateau is observed for O2(Li + x) during its first charge in the voltage range 4.5-4.6 V, similar to the one observed by Paulsen *et al.*<sup>41</sup> in Li<sub>2/3</sub>(Li<sub>1/6</sub>Mn<sub>5/6</sub>)O<sub>2</sub> and Li<sub>2/3</sub>(Co<sub>1/18</sub>Mn<sub>17/18</sub>)O<sub>2</sub>.

CVs recorded on the cells Li/O2(Li + x) and Li/O2(Li) are shown in Fig. 3. The CV of the O2(Li) compound (Fig. 3a) shows only one oxidation peak centered around 4.2 V in the first anodic scan, whereas two oxidation/reduction peaks are seen with almost equal areas in the subsequent cathodic as well as anodic scans. The CV profiles are in accordance with the charge/discharge cycling performance of the respective cells with the Li anode. The single oxidation peak for the first anodic scan is ascribed to the oxidation of Ni<sup>2+</sup> in the lattice with 1/3 mol Li extraction as per Eq. 1. The observed two peaks in the subsequent cathodic and anodic scans are associated with the redox couple of Ni<sup>2+</sup>/Ni<sup>3+</sup> or Ni<sup>2+</sup>/Ni<sup>4+</sup> (4 V) and Mn<sup>3+</sup>/Mn<sup>4+</sup> (3 V). The peak at 4.2 V noted during the first oxidation gets shifted by 0.25 V to the lower voltage side in the

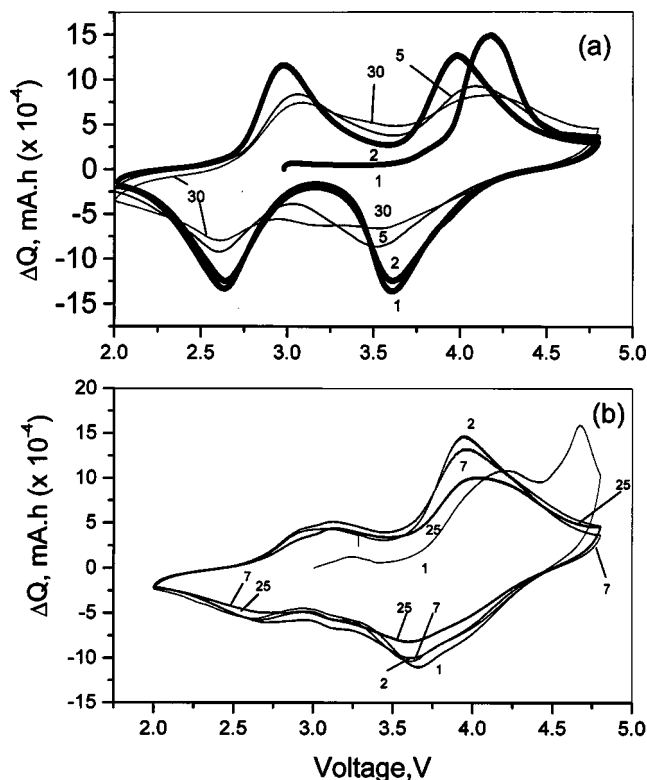


**Figure 3.** Cyclic voltammograms of the cathode (a)  $\text{Li}_{2/3}(\text{Ni}_{1/3}\text{Mn}_{2/3})\text{O}_2$  [O2 (Li)] and (b)  $\text{Li}_{(2/3+x)}(\text{Ni}_{1/3}\text{Mn}_{2/3})\text{O}_2$  [O2 (Li + x)] for various cycles recorded at a scan rate of 0.052 mV/s between 2.0 and 4.7 V. Li used as reference and counter electrode. Cycle numbers are indicated.

second cycle. These CV profiles are in agreement with the differential capacity vs. voltage plots derivable from low current charge/discharge profiles reported by Paulsen *et al.*<sup>1,2</sup>

For the O2 (Li + x) compound, three distinct oxidation peaks are seen in the first anodic scan, a minor peak at 3.25 V which almost merges with the second at 4.2 V and an irreversible peak centered at 4.65 V (Fig. 3b). Subsequent cathodic and anodic scans show only peaks, similar to O2 (Li). However, for the O2 (Li + x), the relative areas under the peaks are different, the higher voltage region (3.65–3.95 V) showing larger area. Further, the peaks observed at 3.25 and 4.2 V during the first oxidation get shifted by 0.15 and 0.25 V, respectively, to the lower voltage side in the second cycle and remain almost unaltered in the subsequent cycles. Also, the relative areas of the peaks remain the same. The first anodic peak at 3.25 V in O2 (Li + x) can be ascribed to the oxidation of  $\text{Mn}^{3+}$  ions in the lattice (reverse of Eq. 2). However, since its intensity is small compared to the main 3.95 V oxidation peak, we can assume that only smaller number of  $\text{Mn}^{3+}$  ions contribute to it whereas the majority of these participate in the oxidation processes, along with  $\text{Ni}^{2+}$  ions at the 4 V region. This assumption is due to the fact that changes in the deintercalation/intercalation voltage can occur due to the Ni-Mn, Ni-Co, or Ni-Co-Mn ion interactions in the layer compounds as has been experimentally observed recently in  $\text{Li}_{0.6}(\text{Co}_{0.5}\text{Mn}_{0.5})\text{O}_2$ ,<sup>42</sup>  $\text{Li}(\text{Co}_{1-2x}\text{Ni}_x\text{Mn}_x)\text{O}_2$ ,  $x = 1/4$  and  $3/8$ ,<sup>43</sup> and  $x = 1/3$ <sup>44</sup> and in  $\text{Li}(\text{Ni}_{1/2}\text{Mn}_{1/2})\text{O}_2$ ,<sup>45,46</sup> and is supported by recent theoretical calculations.<sup>47</sup> We note that the average valency of Mn in O2 (Li + x) is 3.5 before anodic oxidation, and increases toward 4.0 V at the onset of anodic cycle. This is exactly analogous to the spinel,  $\text{LiMn}_2\text{O}_4$  exhibiting 4 V behavior for Mn valency  $\geq 3.5$  and 3 V behavior for Mn valency  $< 3.5$ . Thus LiI treatment of O2 (Li) and the irreversible peak observed at 4.65 V during the

first cycle in O2 (Li + x), somehow seem to shift the main redox potential of O2 (Li + x) to 4 V region.

The CV profile of the O2 (Li + x) phase is qualitatively different from that of O2 (Li) as can be seen in Fig 3. Also, for both the compounds, the profile of the first anodic scan is distinctly different from the subsequent ones. The shifting of the first oxidation peak at 4.2 V to the lower voltage side by 0.25 V in both O2 (Li) and O2 (Li + x) in the respective second and subsequent cycles may be due to the initial activation processes of the electrode material and/or due to the reduction of stacking faults associated with the T2 to O2 phase transition in the compounds.<sup>8,9</sup> The appearance of the irreversible and sharp peak at 4.65 V in the first anodic scan observed in O2 (Li + x) is not seen in O2 (Li). This irreversible peak is seen as irreversible plateau in the voltage profile of O2 (Li + x) during its first charge. Similar irreversible plateau is observed by Paulsen *et al.*<sup>41</sup> in O2-type  $\text{Li}_{2/3}(\text{Li}_{1/6}\text{Mn}_{5/6})\text{O}_2$  and  $\text{Li}_{2/3}(\text{Co}_{1/18}\text{Mn}_{17/18})\text{O}_2$  and by us in  $\text{Li}_{2/3}(\text{Co}_{0.15}\text{Mn}_{0.85})\text{O}_2$ .<sup>7</sup> These materials are shown to have stacking faulted O2-type structure.<sup>38</sup> The reasons for this are not known at present. Contribution of electrolyte decomposition for this peak cannot be ruled out due to the high potential. But the irreversible nature of the peak which does not appear in the subsequent cycles reveals that the profile is inherent to O2 (Li + x). The reduction in intensity observed in the CV profiles during 5–25 (or 30) cycles for both the compounds is possibly due to the electrolyte decomposition due to the fact that the upper voltage limit for the measurement was 4.8 V. Therefore, we conclude that the compound O2 (Li + x) shows an improved performance over O2 (Li) by way of better capacity retention on charge discharge cycling and an improved rate capability.

**Electrochemical impedance spectroscopy.**—EIS is a powerful tool to identify the kinetics of lithium intercalation/deintercalation into the electrodes.<sup>10–28</sup> The measured impedance of the electrochemical cell is a collective response of kinetic processes occurring in the electrode. The Li intercalation and deintercalation into the positive electrode materials is normally modeled as a multistep process which involves and reflects a serial nature of many processes occurring during intercalation/deintercalation. The main challenge for the interpretation of impedance data is to identify the proper equivalent circuits which are more consistent with the processes occurring in the electrode envisaged by parallel physicoelectrochemical investigations. There are different models to explain the impedance response of the intercalation system.<sup>10–28</sup> Theoretical analysis of complex impedance response for lithium insertion into thin  $\text{WO}_3$  film has been performed by Ho *et al.*<sup>10</sup> Modeling of the impedance response of the cell with  $\text{LiCoO}_2$  as positive electrode material was reported by Thomas *et al.*<sup>11</sup> The general nature of most of these models is to account and explain the Li-ion migration through the surface film, charge-transfer through the electrode/electrolyte interface, and the solid-state diffusion of Li in the compound.<sup>12–28</sup> The involvement of material conductivity on the impedance response has also been addressed in some reports.<sup>16–19</sup> In the present study, the possible and experimentally visualized processes which are at par with other observations are (i) a resistive component ( $R_e$ ) arising from the electrolyte resistance and cell components, (ii) the double layer (dl) capacitance of the surface film and the associated impedance ( $C_{sf}$  and  $R_{sf}$ ), (iii) the impedance associated with the bulk of the active material and the capacitance associated with it ( $R_b$  and  $C_b$ ), (iv) the charge transfer (electron transfer) resistance of the intercalation reaction and the capacitance of the dl ( $R_{ct}$  and  $C_{dl}$ ), and (v) a Warburg contribution ( $W_o$ ; finite length Warburg open-circuit terminal) which is characteristic of the Li ion diffusion through the bulk of the active material.

Figures 4 and 5 represent the Nyquist plots measured on the cell with O2 (Li + x) (fifth charge) and O2 (Li) (second charge), respectively, as cathodes at different cell potentials [lithium content x in  $\text{Li}_x\text{MO}_2$  (M =  $\text{Ni}_{1/3}\text{Mn}_{2/3}$ )] during the lithium deintercalation cycle. For each impedance measurement, the cells were galvanostatically

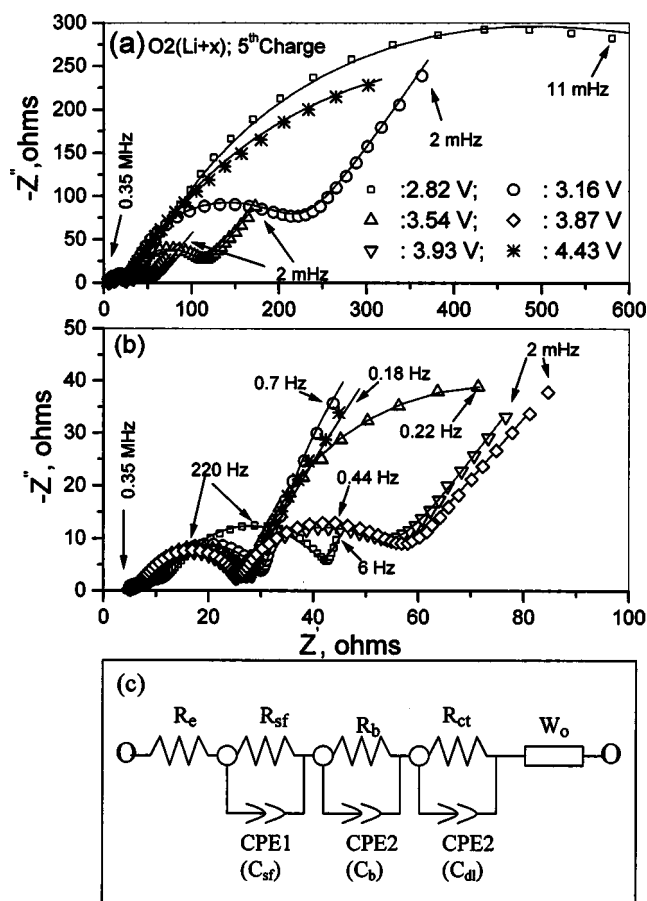


**Figure 4.** Family of Nyquist plots for O<sub>2</sub>(Li + x) electrode at different voltage (under open circuit voltage (OCV) conditions) during the course of fifth charging (a) for full range of  $Z'$  values, (b) expanded view of the low  $Z'$  region in (a). Voltages are indicated and the respective symbols are common to (a) and (b). The symbols represent experimental data and the continuous line represents the fitting with equivalent circuit; (c) the equivalent circuit used to fit the experimental data.

statically charged ( $\sim C/20$  rate) for a known time and left in the open-circuit condition for 3 h to relax the cell potential ( $E$ ) to a stable value. The impedance spectra were then measured at open-circuit condition. The spectra of O<sub>2</sub>(Li + x) consist of two overlapped semicircles in the high- to medium-frequency range (0.35 MHz to 20 Hz), a broad semicircle at the low frequency (20 Hz to 20 mHz), and Warburg impedance at very low frequency (20-2 mHz). It may be noted that the high frequency as well as the medium frequency semicircles at the beginning and end of deintercalation are not clearly seen in Fig. 4 and 5 due to the large  $Z'$  value of the low frequency semicircle. The expanded views of the low  $Z'$  domains of Fig. 4a and 5a are shown in Fig. 4b and 5b, respectively. The nature of variation of the shape and  $Z'$  values in the high-to-medium frequency region of the impedance spectra for both the compounds are almost similar. Both show two overlapped semicircles, the shape of which do not change much with cell voltage during a single titration. However, the impedance response of the freshly prepared cell during its first charge cycle, shown in Fig. 6, is different from that observed in cells subjected to second and subsequent charge/discharge cycles. The high frequency semicircle is absent or masked by the medium frequency semicircle for the fresh cells and become distinguishable only after starting the deintercalation process ( $>3.8$  V) for both O<sub>2</sub>(Li + x) and O<sub>2</sub>(Li) as can be seen in Fig. 6. Further, the gradual decrease in the  $Z'$  values of the high to medium frequency contribution seen during the first charge cycle is absent in the cycled cells.

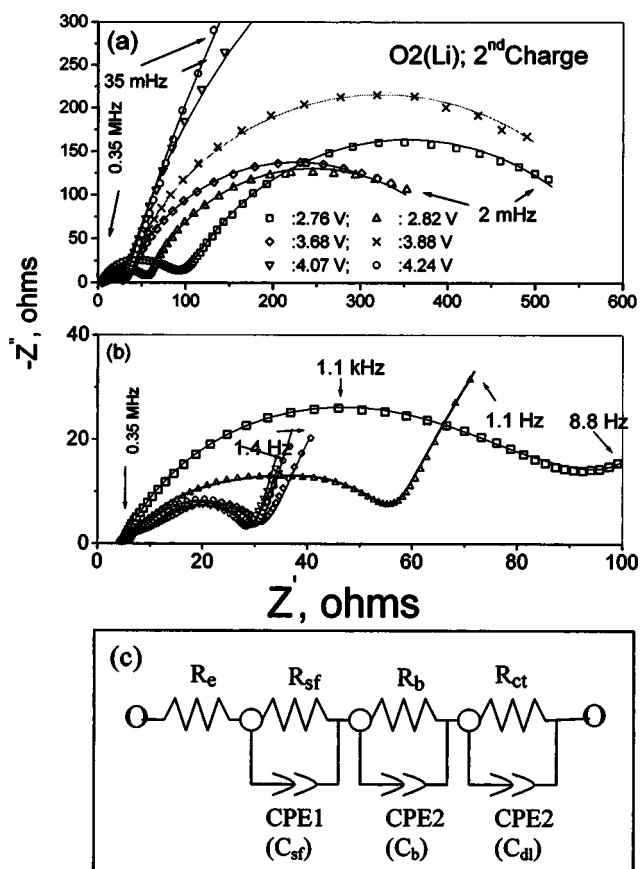


**Figure 5.** Family of Nyquist plots for O<sub>2</sub>(Li) electrode at different voltages (under OCV conditions) during the course of second charging (a) for full range of  $Z'$  values, (b) expanded view of the low  $Z'$  region in (a). (c) the equivalent circuit used to fit the experimental data. The voltages are indicated. The symbols represent the experimental data and the continuous lines represent the fitting with equivalent circuit.

Depending on the measurement conditions like voltage (or lithium content  $x$ ), cycle number, and frequency range, one or more of the impedance contributions as mentioned above may be absent and/or indistinguishable in the frequency range of measurement as can be seen from Fig. 4, 5, and 6. For instance, the Warburg contribution in O<sub>2</sub>(Li + x) disappears at the end of deintercalation (4.43 V) (Fig. 4a) and the impedance plots of O<sub>2</sub>(Li) do not show the low frequency Warburg contribution for the full voltage range (second charge, 2.5-4.6 V) of measurement (Fig. 5a).

The impedance spectra of Fig. 4 and 5 were analyzed using physical processes that could be represented by resistive/capacitive combination. The relevant equivalent circuits are shown in Fig. 4c and 5c, respectively. The respective circuit elements were deduced by fitting the experimental data points with the equivalent circuit. To compensate for the nonhomogeneity of the composite electrode system (reflected as depressed semicircle in the impedance response), a constant phase element (CPE) is used in place of capacitor to model the data as shown in Fig. 4c and 5c. The impedance of the CPE is defined as  $Z = 1/B(j\omega)^n$  where  $j = \sqrt{-1}$ ,  $\omega$  is the angular frequency,  $B$  and  $n$  are constants. The CPE become an ideal capacitor (C) when  $n = 1$  and hence  $B = C$ . The values of  $n$  observed in the present study range from 0.7-1.0. In Fig. 4 and 5, the continuous line represents the fitting as per the equivalent circuit whereas the symbols denote the experimental data as a function of frequency for a given voltage. For the spectra which do not contain the Warburg contribution (and/or other contributions), the respective circuit ele-

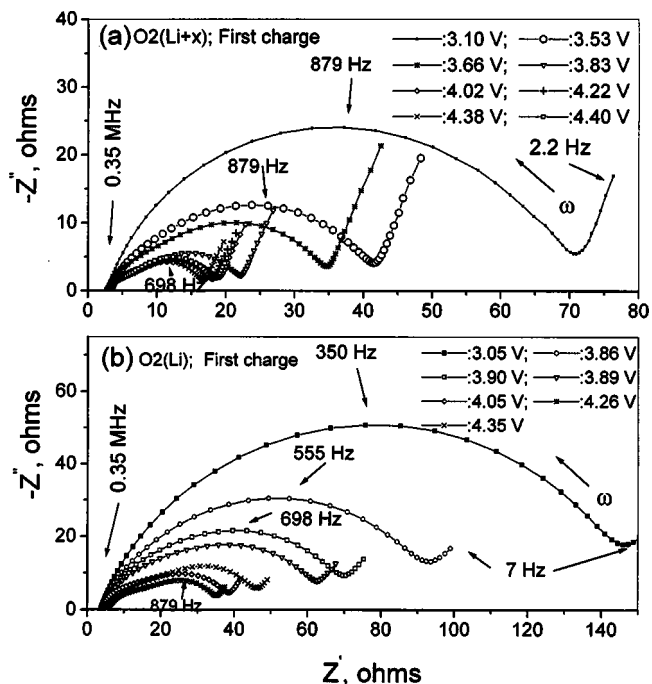


**Figure 6.** Variation of the high- to medium-frequency range of the Nyquist plots during the first charging cycle. (a) O<sub>2</sub>(Li + x), (b) O<sub>2</sub>(Li). Voltages are indicated.  $\omega$  is the frequency.

ments were removed from the assumed model to fit the data. As can be seen the experimental points fitted well with the equivalent circuit response.

The charge-transfer resistance ( $R_{ct}$  associated with the low frequency semicircle) extracted from Nyquist plots and equivalent circuits for the cells with O<sub>2</sub>(Li + x) (first, second, and fifth charge and discharge sequences) and with O<sub>2</sub>(Li) (first and second cycle sequences) as a function of cell voltage ( $E$ ) during intercalation/deintercalation are shown in Fig. 7. The  $R_{ct}$  values at the beginning and end of Li intercalation for O<sub>2</sub>(Li) where the low frequency semicircle was not completely seen, were determined by completing

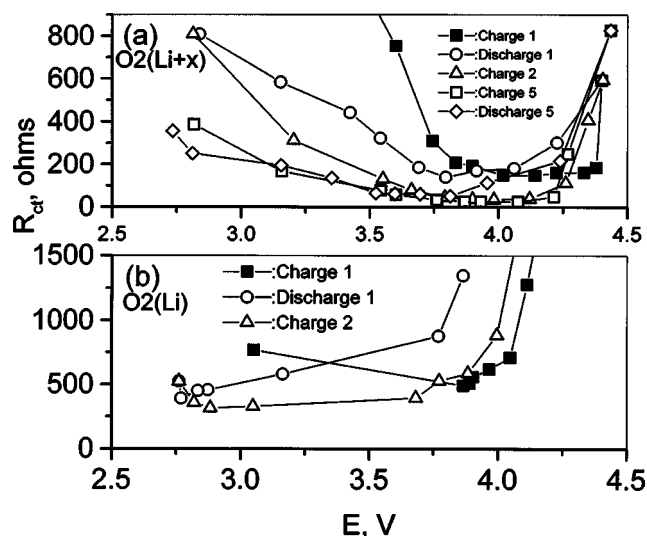


**Figure 7.** Voltage dependence of  $R_{ct}$  for different charge and discharge cycles (a) for O<sub>2</sub>(Li + x), (b) for O<sub>2</sub>(Li). Cycle numbers and mode of operation are indicated. The error in fitting for  $R_{ct}$  is <1% and is within the size limit of the symbols.

the arc of the respective impedance spectra. In the case of O<sub>2</sub>(Li + x), the  $R_{ct}$  value for the freshly fabricated cell is high (1750  $\Omega$ ; cell voltage, 3.10 V). There is a rapid decrease in the  $R_{ct}$  value as deintercalation starts and falls to 750  $\Omega$  at 3.60 V.  $R_{ct}$  passes through a broad minimum in the voltage range 3.6–4.3 V (corresponding to  $x = 0.8$ –0.40 in Li<sub>x</sub>MO<sub>2</sub>) and then increases again to high values at the end of deintercalation (593  $\Omega$  at 4.40 V; Fig. 7). For the subsequent Li intercalation (first-discharge process), the  $R_{ct}$  value gradually decreases below 3.7 V and approaches a value of 810  $\Omega$  at 2.81 V. A gradual decrease in the  $R_{ct}$  values for the first discharge and subsequent charge/discharge cycles are seen due to the activation of the electrode for charge transfer with the onset of current flux. The activation of the electrode surface can be brought about by different ways: an effective electrolyte penetration into the composite electrode resulting in more surface of the active mass exposed to the electrolyte, change in the surface layer thickness due to the current flux as discussed by Levi *et al.*,<sup>14</sup> replacement of the pristine surface film covering the electrode by more active one by the interactions between solution species, and the active mass assisted by the current flux. The identical values of  $R_{ct}$  observed for the fifth charge and discharge cycles for O<sub>2</sub>(Li + x) reveals that the initial formation (activation) of the electrode is complete by the fifth cycle and the increase in its values at the end of intercalation is also minimal. The stable  $R_{ct}$  values observed for the fifth cycle in the range 3.7–4.1 V ( $x = 0.4$ –0.8) are of the order of 20–30  $\Omega$ . A similar variation of  $R_{ct}$  with voltage was reported for the well-known cathodes, Li<sub>x</sub>NiO<sub>2</sub>,<sup>12</sup> Li<sub>x</sub>Ni<sub>0.8</sub>Co<sub>0.2</sub>O<sub>2</sub>,<sup>14</sup> and LiMn<sub>2</sub>O<sub>4</sub>.<sup>12,13</sup> However, a monotonic decrease in  $R_{ct}$  values was observed for Li<sub>x</sub>CoO<sub>2</sub> with increase in voltage (decrease in  $x$ ).<sup>12,15</sup> Also, the plateau-like minima in the  $R_{ct}$  values reported for the above well-known cathodes were found to be different: for LiNiO<sub>2</sub>  $\sim$ 500  $\Omega$  (3.7–4.0 V),<sup>12</sup> for LiMn<sub>2</sub>O<sub>4</sub>  $\sim$ 100  $\Omega$  (3.95–4.15 V),<sup>13</sup> and for Li<sub>x</sub>Ni<sub>0.8</sub>Co<sub>0.2</sub>O<sub>2</sub>  $\sim$ 10  $\Omega$  (3.7–4.1 V).<sup>14</sup>

Present results show that the variation of  $R_{ct}$  of the O<sub>2</sub>(Li) is strikingly different from that of O<sub>2</sub>(Li + x). For the former, the  $R_{ct}$  shows a value of 770  $\Omega$  for the freshly prepared cell (3.05 V), decreases to 490  $\Omega$  at the beginning of deintercalation (3.80 V) and gradually increases to a very high value as the Li content decreases at the end of deintercalation (2720  $\Omega$  at 4.26 V, not shown in Fig 7b). On discharge, the  $R_{ct}$  values decrease at a faster rate at the beginning ( $E > 3.8$  V), show a minimum of 390  $\Omega$  at 2.77 V, and then increase to 525  $\Omega$  at the end of discharge ( $E = 2.75$  V). For the second charge cycle in the O<sub>2</sub>(Li),  $R_{ct}$  value initially decreases on deintercalation (from 525  $\Omega$  at 2.75 V to 317  $\Omega$  at 2.88 V) and is stable up to 3.7 V with a value of  $\sim$ 300  $\Omega$ . As the electrode approaches the stage of full deintercalation,  $R_{ct}$  increases rapidly to a value of 4730  $\Omega$  at 4.24 V ( $x = 0.33$ , not shown in Fig 7b). It can be seen that after the initial formation, the increase in  $R_{ct}$  of the electrode at the end of discharge (2.75 V and  $x \sim 1.0$ ) is minimal and is similar for both systems, though their absolute values are different. The value corresponding to the broad minimum observed for  $R_{ct}$  in the voltage range 2.75–3.9 V ( $x = 0.5$ –1.0) for O<sub>2</sub>(Li) is almost one order of magnitude larger than that obtained for the cell with O<sub>2</sub>(Li + x) (Fig. 7a and b). This may be caused by differences in the nature of surface film covering these compounds even though we have used identical cell parameters (electrode thickness, area, and processing conditions) for both the systems. The lithiation process with LiI might have changed not only the morphology of particle of O<sub>2</sub>(Li + x) but also its electronic structure, with a more active surface facilitating easy charge transfer. However, it can be mentioned that the high  $R_{ct}$  values in O<sub>2</sub>(Li) indicate sluggish kinetics at the interface which in fact is reflected in the cell kinetics. The observed higher current rate capability of the O<sub>2</sub>(Li + x) can be understood as due to the better charge transfer kinetics. The increase in  $R_{ct}$  of the electrodes either in completely intercalated state (2.7 V) for O<sub>2</sub>(Li + x) and deintercalated state for both O<sub>2</sub>(Li

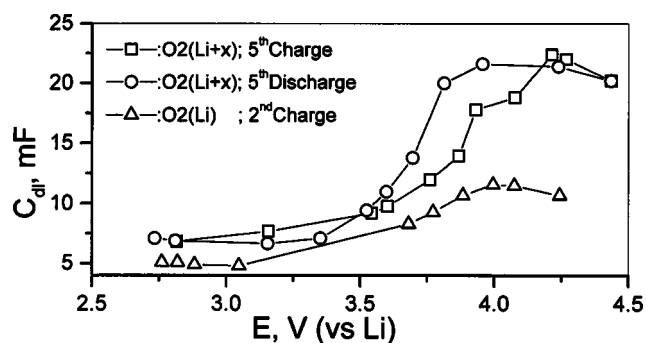


**Figure 8.** Voltage dependence of  $C_{dl}$  for O2 (Li + x) for the fifth charge and discharge cycles and for O2 (Li) for the second charge cycle. Error in fitting is  $<1\%$  and is within the size limit of the symbols.

+ x) (4.4 V) and O2 (Li) (4.25 V) are in accord with the expected nature for charge transfer kinetics as observed and discussed by Aurbach and his co-workers for other cathodes  $\text{Li}_x\text{NiO}_2$ ,<sup>12</sup>  $\text{Li}_x\text{Mn}_2\text{O}_4$ ,<sup>12,13</sup> and  $\text{Li}_x\text{Ni}_y\text{Co}_{(1-y)}\text{O}_2$ .<sup>14</sup> However, the O2 (Li) shows a sudden increase in  $R_{ct}$  values as it reaches the fully deintercalated (charged) state compared to O2 (Li + x). This may be due to the inefficient charge transfer in the O2 (Li). This can be seen from the CV profiles ( $\Delta Q$  vs. V shown in Fig. 3) of the compounds where significant contribution of charge transfer is observed for O2 (Li + x) as compared to O2 (Li) as the cell approaches 4.6 V. Such an inefficient nature of charge transfer in O2 (Li) can overshoot the cell potential to a higher value from its equilibrium potential. The lower equilibrium potential observed for the cell with O2 (Li) (4.25 V) compared to O2 (Li + x) (4.4 V) after charging them to 4.6 V consolidate this argument. Further, it can be seen from the voltage profiles of the cells during their charge/discharge processes (Fig. 2) that the O2 (Li) shows a very high ohmic drop (4.6 to  $\sim 4.0$  V) at the onset of discharge while the voltage profile is continuous from 4.4 V for O2 (Li + x). Alternatively, such a variation in  $R_{ct}$  in O2 (Li) can also be caused by the difference in Li-ion diffusion inside the bulk. Since the charge transfer at the interface is also controlled by the availability of  $\text{Li}^+$  ions at the surface, a possible change in diffusion coefficient at the end of deintercalation can also bring such a difference in  $R_{ct}$  for O2 (Li).

The dl capacitance ( $C_{dl}$ ) extracted from the impedance data and curve fitting are shown in Fig. 8. As can be seen the  $C_{dl}$  values for O2 (Li + x) (fifth cycle, charge, and discharge sequence) and for O2 (Li) (second charge sequence) show almost similar behavior with change in voltage (or lithium content, x). On lithium depletion (increase in cell voltage), the  $C_{dl}$  shows an increase followed by a saturation behavior at the end of charge [10 mF for O2 (Li) and 20-23 mF for O2 (Li + x)]. For the full range of voltage, the  $C_{dl}$  values lie in the range of 5-23 mF. The O2 (Li + x) have higher  $C_{dl}$  values possibly due to the more active surface brought by the LiI treatment. Therefore, a direct comparison of the absolute values of  $C_{dl}$  for both the compounds may not have significance. But the relative difference in their variation with voltage are of relevance. It can be seen that the  $C_{dl}$  for O2 (Li + x) shows a rapid increase with voltage around 3.7 V. Since this region coincides with the voltage range (3.7-4.2 V) of the observed broad minima in  $R_{ct}$ , it can be thought that an easy reduction in thickness of the dl in O2 (Li + x) by the active charge transfer processes. The nature of variation of  $C_{dl}$  vs. voltage for both O2 (Li) and O2 (Li + x) in the present study is similar to that reported for  $\text{Li}_x\text{Ni}_y\text{Co}_{(1-y)}\text{O}_2$  ( $y = 0.2$  and  $0.25$ ),<sup>14,20</sup> including the range of  $C_{dl}$  values (a few millifarad) for the full voltage range.

As mentioned earlier, the main change observed in the impedance spectra as Li deintercalation proceeds for O2 (Li + x) is that the Warburg contribution which is prominent at the early stages

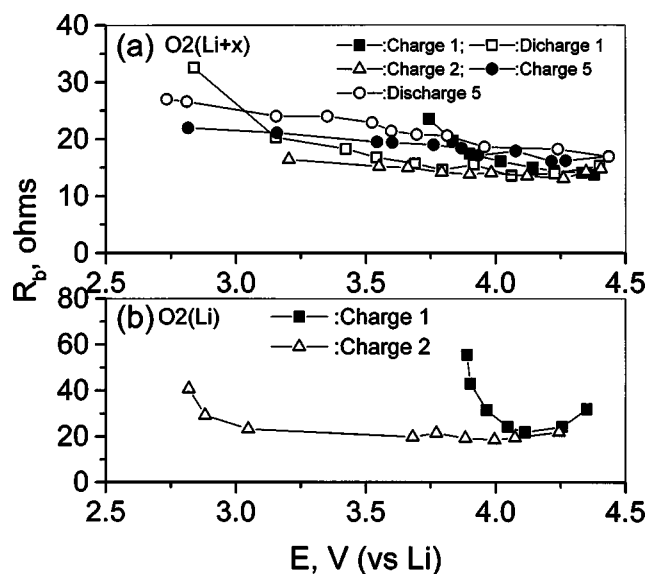


**Figure 9.**  $R_b$  values as a function of voltage for different charge and discharge cycles. (a) O2 (Li + x) and (b) O2 (Li). The error in fitting  $R_b$  is 2 to 6% and is within the size limit of the symbols.

(3.15-4.3 V; all plots are not shown in Fig. 4) of deintercalation become indistinguishable at the end of deintercalation ( $>4.3$  V). Such type of behavior in the low frequency side of the impedance response at the beginning and end of deintercalation is commonly observed in studies on other cathodes as well.<sup>12,14,16,23</sup> This indicates that at the early stage of deintercalation, the kinetics of the electrode processes is controlled by the diffusion processes in the low frequency region and by the charge transfer in the high frequency region. At the end of deintercalation, the electrode kinetics is controlled by the charge transfer contribution. The reason for this periodical change can be understood from the fact that the  $R_{ct}$  value increases enormously at the end of deintercalation.

Impedance response of most of the composite electrodes shows a single semicircle at the high frequency and the contribution is mostly treated as arising due to the surface film at the active material surface.<sup>12,13,22,26,27</sup> Alternatively, the high frequency contribution is also addressed as due to the porous nature of the composite electrode comprising active material, conducting carbon, and the organic binder.<sup>11,21,28,32</sup> A comparison of impedance response of thin film and composite electrode of  $\text{LiCoO}_2$  by Dokko *et al.*<sup>28</sup> shows that the high frequency contribution is due to the porous nature of the electrode. Since the cell has Li metal as anode, the possibility of surface film at the Li/electrolyte interface as observed in the polymer Li-ion battery<sup>18,19</sup> cannot be ruled out. The impedance response of the presently studied compounds shows two semicircles at the high frequency side. The variation of the impedance associated with the slightly depressed medium frequency semicircle ( $R_b$ ) with voltage for different charge/discharge cycles is shown in Fig. 9. The freshly prepared cells of both O2 (Li) and O2 (Li + x) (as well as the fully discharged cell after first cycle) do not show the indication of two well-defined semicircles at the high frequency side (first charge curves shown in Fig. 6). This is due to the overlapping of both semicircles owing to closeness in the time constants associated with these processes. Hence the extracted  $R_b$  values from such overlapped semicircles are excluded in Fig. 9. The nature of variation of  $R_b$  for O2 (Li + x) and O2 (Li) is similar except a slight difference in their absolute values. For the cell with O2 (Li + x), the  $R_b$  values gradually decrease on deintercalation reaching a value of 15  $\Omega$  at the end of the first charge (4.40 V). During the first discharge, the  $R_b$  value of 10  $\Omega$  remains stable in the voltage range 3.7-4.4 V, and increases to 15-18  $\Omega$  in the range of 3.1-3.6 V. For the second

charge the  $R_b$  value ( $\sim 13 \Omega$ ) remains constant up to the end of charging (4.41 V). For the fifth charge and discharge cycle,  $R_b$  shows consistently low values (17-27  $\Omega$ ) in the entire composition range, but show a minor periodic variation with change in voltage for the full charge/discharge cycle. For the cell with O2 (Li), the  $R_b$  decreases gradually during the first charge to 22  $\Omega$  at 4.11 V and then increases to a value of 32  $\Omega$  at the end of charge (4.35 V). For the second charge,  $R_b$  shows a gradual variation from 41  $\Omega$  at 2.82 V to a value of 22  $\Omega$  in the charged state (4.24 V). It can be seen from Fig. 9 that both compounds show a periodical variation in their  $R_b$  values and their absolute values lie in the same range after the formation cycle.

A periodical variation in the impedance values of the semicircle in the same frequency range as found in the present study has also been observed in other intercalation compounds<sup>14</sup> and the contribution is mostly treated as arising due to the surface film.<sup>12-15</sup> The development of surface film on the as-prepared cathodes like LiCoO<sub>2</sub> and LiNiO<sub>2</sub> established by Fourier transform infrared spectroscopy (FTIR) and other techniques reveals that the active mass of the electrode is covered with surface films, mostly composed of Li<sub>2</sub>CO<sub>3</sub>.<sup>12,48</sup> In contact with the electrolyte solution, these surface films may be replaced by more complex surface species and/or films which originate by the complicated reaction of the electrode material with the electrolyte.<sup>12,48</sup> Considering the fact that the oxidation potentials of the solvents constituting the electrolyte are higher than the upper voltage limit of the experiment and the nature of reaction products, Aurbach *et al.*<sup>12</sup> assumed that these products were formed at the anode in the cell and precipitated on the cathode through the solution. This assumption was supported by the observation that the surface films are formed only after several charge/discharge cycles.<sup>12</sup> If the observed second semicircle in the impedance spectra is due to surface film, its value is expected to be more in the charged state where the cell potential is high and hence the decomposition of electrolyte (if any) may be maximal. But in the present case, it is observed that the  $R_b$  is maximum in the discharged state and has a minimal value in charged state. This indicates that the origin of the second semicircle is something else other than the development of surface film, possibly due to the change in bulk properties (electronic conductivity, diffusion of ions, etc.) of the cathode material. Note the drastic change in conductivity predicted for the Li<sub>x</sub>MO<sub>2</sub> (M = Co) type compounds with a minor change in  $x$  values<sup>49</sup> and experimentally observed as semiconductor-to-metal like transition for  $x > 0.5$  in Li<sub>x</sub>CoO<sub>2</sub><sup>50,51</sup> and is shown to be applicable to mixed oxides with the formula Li<sub>x</sub>(Ni<sub>y</sub>Co<sub>1-y</sub>)O<sub>2</sub>,  $y = 0.8$ ,<sup>52</sup> 0.75,<sup>17</sup> 0.3,<sup>53</sup> 0.1.<sup>54</sup> The compounds, O2 (Li) and O2 (Li +  $x$ ) presently studied also have a similar crystal structure and it is reasonable to expect a similar type of conductivity variation with change in  $x$ . The periodical variation of the  $R_b$  values with  $x$  (or voltage) during charge/discharge may arise from their change in electronic conductivity as  $x$  varies. This is due to the variation in the ratio of concentration of the ions, Mn<sup>3+</sup>/Mn<sup>4+</sup> and Ni<sup>2+</sup>/Ni<sup>4+</sup> or Ni<sup>2+</sup>/Ni<sup>3+</sup> ions even though we do not expect a drastic variation in the electronic conductivity. Also, the involvement of the Li/electrolyte interface as observed in polymer Li-ion batteries,<sup>18,19</sup> cannot be ruled out as a possible contribution to  $R_b$  because the cells have Li metal as anode.

The observed high frequency (0.35 MHz to 5 kHz) semicircle which can be assigned to the surface film resistance ( $R_{sf}$ ) and associated capacitance ( $C_{sf}$ ), is absent or masked by the medium frequency semicircle in the freshly fabricated cell as well as after the discharged state after the first cycle and becomes distinguishable as deintercalation starts as mentioned earlier. The diameter of the semicircle decreases to a minimum and remains constant until the end of deintercalation. This is due to the fact that on subjecting the cell to charge/discharge cycling, the passive surface film, which might have formed on the surface of the electrode by reaction with the electrolyte, may be destroyed and replaced by newly created active surface film by the processes associated with the initial current flux through

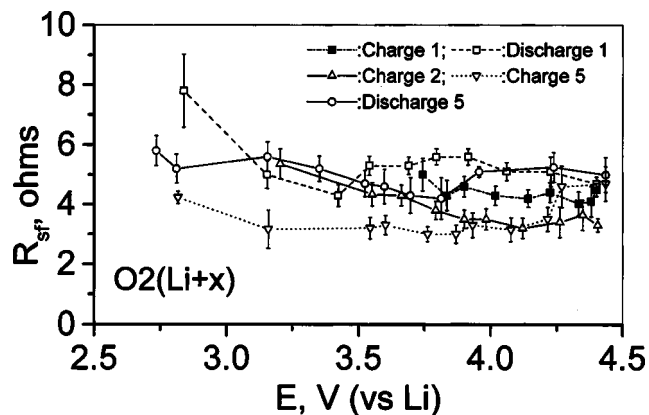
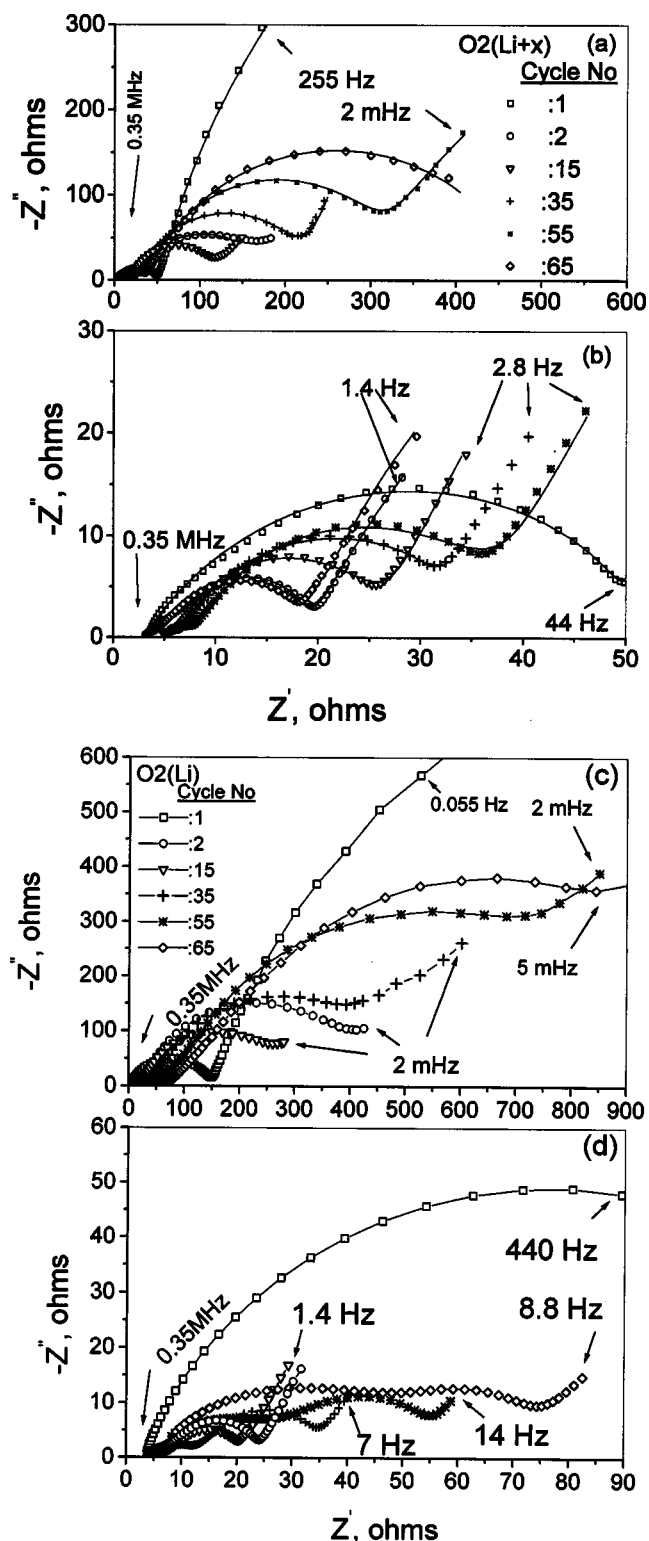


Figure 10.  $R_{sf}$  values as a function of voltage for different charge and discharge cycles for the compound O2 (Li +  $x$ ). Error bars are indicated.

the interface. The initial activation of the surface film, the change-over of the passive film to the active one, can be visualized by monitoring the impedance spectrum during the process of first deintercalation as a gradual decrease in the diameter of the high frequency semicircle as can be seen in Fig. 6. The diameter of the high frequency semicircle remains unchanged in the full voltage range for the formed electrodes O2 (Li +  $x$ ) and O2 (Li) in the subsequent charge/discharge cycles. This can be seen from Fig. 10, where the  $R_{sf}$  values for the O2 (Li +  $x$ ) are plotted as a function of voltage for different cycles (also note the stable values of  $R_b$  for the fifth charge/discharge cycle). After the second charge cycle, the  $R_{sf}$  values are stable in the voltage range (2.5-4.6 V) for a single titration (charge or discharge sequence) indicating that the surface film on the compound O2 (Li +  $x$ ) is stable with low resistance (Fig. 10). A similar stable value of the  $R_{sf}$  for the full voltage range was also reported for Li<sub>x</sub>NiO<sub>2</sub>.<sup>12</sup> The stable value of  $R_{sf}$  with change in voltage (composition  $x$ ) also indicates that the reactivity of the electrode material in the charged state with the electrolyte and associated decomposition is minimal for O2 (Li +  $x$ ). The  $R_{sf}$  may not have an influential role in the electrode kinetics for a single charge or discharge cycle. However, the evolution of surface film on the electrode on repeated charge/discharge cycling may influence the performance of the electrode material.

The formation of the surface film is known to play a decisive role in the performance of the electrodes in Li-ion cells. The formation of such a film in graphite<sup>12,26,27,48</sup> and other intercalation compounds are known to act as a protective coating which improves their performance.<sup>12,13,26,27,48</sup> The nature of surface film, which covers the active mass may provide a measure of its particle to particle contact. A mass deposition of the surface film on the electrode surface may end up as a destructive film, which would slow down the electrode kinetics and hence its performance. The influence of surface film formation on the performance of LiMn<sub>2</sub>O<sub>4</sub> cathode has been studied for half cells with a Li metal anode<sup>12</sup> and in plastic Li cells (with a polymer electrolyte and Li anode).<sup>19</sup> It was shown that the increase in resistance associated with the surface film with repeated charge/discharge cycling which deteriorates the performance can be monitored by impedance spectroscopy. Therefore, the deterioration of the electrode material and its interface with cycling can be quantitatively analyzed by monitoring the impedance spectra of the cells with different cycle number. Figure 11 shows the impedance spectra measured on cells with O2 (Li +  $x$ ) and O2 (Li) after subjecting them to different number of charge/discharge cycles at room temperature.

The spectra were measured after cycling them at C/5 rate to the desired cycle number and then charging to 3.8 V (vs. Li) followed by holding at 3.8 V for 0.5 h. This charging voltage corresponds to  $x$  in the range 0.5-0.6 in Li<sub>x</sub>MO<sub>2</sub> where different contributions for the impedance response of the cell are distinguishable due to low  $Z'$



**Figure 11.** Family of Nyquist plots measured after different number of cycles (hold at 3.8 V for 0.5 h after each cycle). (a) Full range of impedance response for O<sub>2</sub>(Li + x), (b) expanded view of the low Z' region from (a), (c) for O<sub>2</sub>(Li), and (d) expanded view of the low Z' region from (c). Cycle numbers are indicated. The symbols represent the experimental data and the continuous line represents the fitting with equivalent circuit shown in Fig. 4c and 5c.

values for  $R_{ct}$ . These spectra shown in Fig. 11 demonstrate the change in the electrode kinetics on prolonged charge/discharge cycling which can be correlated to the capacity fading, if any, observed

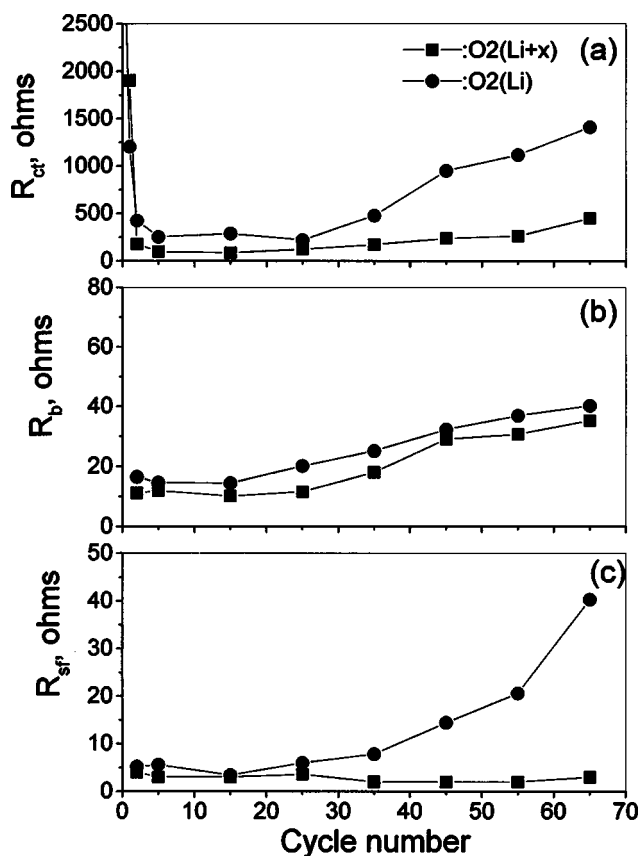


**Figure 12.** Variation of (a)  $R_{ct}$ , (b)  $R_b$ , and (c)  $R_{sf}$  with cycle number O<sub>2</sub>(Li + x) and O<sub>2</sub>(Li) obtained by fitting the impedance response of Fig. 11.

for the compounds, O<sub>2</sub>(Li + x) and O<sub>2</sub>(Li). The variation of different resistive components obtained by fitting the impedance spectra to the equivalent circuit model described in Fig. 4c and 5c are shown in Fig. 12 as a function of cycle number.  $R_{ct}$  decreases drastically in the first two cycles for both compounds, indicating the electrode formation/surface modification, and remains almost unchanged with a value of  $\sim 250 \Omega$  for O<sub>2</sub>(Li) and  $\sim 100 \Omega$  for O<sub>2</sub>(Li + x) up to 25 cycles. Thereafter, the  $R_{ct}$  values for the cell with O<sub>2</sub>(Li) increase drastically with cycling and reach 1400  $\Omega$  after 65 cycles.

On the other hand, the variation for the cell with O<sub>2</sub>(Li + x) is minimal and reaches 450  $\Omega$  after 65 cycles. The  $R_b$  value for both the compounds increases slowly with cycle number. The rate of increase of  $R_b$  with cycle number is smooth and their respective values are also identical for both the compounds as can be seen from Fig. 12b. This is in accordance with our assignment that  $R_b$  is arising from the bulk of the material. Because both the compounds have similar structure and shown to be stable against cycling,<sup>1-4,8,9</sup> a minor and proportional increase observed in  $R_b$  values with cycling is in support to this assignment. The main observation on the impedance spectra with cycling is that  $R_{sf}$  value for the cell with O<sub>2</sub>(Li) changes drastically after the 25th cycle (6  $\Omega$  at the 25th cycle to 40  $\Omega$  for the 65th cycle) whereas it remains almost invariant (2-4  $\Omega$ ) up to 65 cycles for O<sub>2</sub>(Li + x). As described earlier, the increased contribution for  $R_{sf}$  can be due to the massive surface film formation, the degradation of the composite electrode and due to the deterioration of the Li/electrolyte interface. The possibility of Li/polymer interface deterioration can be ruled out since the change in  $R_{sf}$  with cycle number is different for both compounds. It may be difficult to distinguish the contribution either due to surface film formation or due to the deterioration of the composite electrode

because the resultant effect for both of these processes would be the same, deterioration of electrical connectivity between the active mass and hence an electrical isolation. But the poor interparticle contact is unlikely to be the origin of capacity fading since the liquid electrolyte provides the predominant pathway for charge transfer. Alternatively, the massive surface film formation can hinder the charge transfer and hence contribute to the capacity fading. Therefore, it can be assumed that the increased  $R_{ct}$  and  $R_{sf}$  observed for O2 (Li) is due to the enhanced surface film formation leading to sluggish charge-transfer kinetics at the interface leading to capacity fading.

The nature of variation of  $R_{sf}$  with cycling is in agreement with the observation made by Aurbach *et al.*<sup>12</sup> They found a significant contribution of surface film only after many charge/discharge cycles on graphite as well as on intercalation electrodes like LiCoO<sub>2</sub> and LiMn<sub>2</sub>O<sub>4</sub>. In the case of O2 (Li + x), the  $R_{ct}$  and  $R_b$  values show a slow increase with cycling, especially after 25 cycles, though the  $R_{sf}$  values remain stable. This indicates that the charge-transfer kinetics of the electrode material is influenced by the change in bulk properties together with the surface film formation. The involvement of bulk contribution in the impedance response of the intercalation compounds are indeed observed by others.<sup>16-19</sup>

**Li<sup>+</sup> diffusion coefficient.**—The chemical diffusion coefficient of lithium ( $D_{Li}$ ) in the cathode materials Li<sub>x</sub>MO<sub>2</sub> (M = Co, Ni, Mn) and Li<sub>x</sub>Mn<sub>2</sub>O<sub>4</sub> can be determined by a variety of electrochemical techniques such as GITT,<sup>29-34</sup> PITT,<sup>12,15,35-37</sup> SSCV,<sup>12,15,36</sup> and EIS.<sup>10,15</sup> The  $D_{Li}$  values determined by different techniques show significant discrepancies due to the limitations involved in each measurement. GITT is established to be a reliable technique to determine the  $D_{Li}$  with greater accuracy for compounds with varying composition,  $x$  (or voltage).<sup>29-34</sup>

The GITT is based on chronopotentiometry, where the lithium host electrode with a known composition ( $x$  in Li<sub>x</sub>MO<sub>2</sub>) in thermodynamic equilibrium with Li metal is subjected to lithiation or delithiation by applying a constant current flux ( $I_0$ ) for a limited time period  $\tau$ , at the end of which the compound has a known lithium content,  $x \pm \Delta x$ , depending on the direction of the current. As a result of change in  $x$ , the equilibrium cell voltage ( $E_0$ ) increases (or decreases according to the direction of the current) with time, which is superimposed to an IR drop due to the current flux through the electrolyte and interface. The total change in cell voltage  $\Delta E_\tau$  during the current flux can then be obtained by subtracting the IR drop. After the current is interrupted at  $\tau$ , the cell is allowed to relax to its new steady state potential  $E_s$ , from which the change in the steady-state voltage  $\Delta E_s (= E_s - E_0)$  over the galvanostatic titration can be determined. The procedure is then repeated until the composition interval of interest ( $x$ ) is covered. The diffusion coefficient of lithium ( $D_{Li}$ ) in the compound can be determined by solving Fick's second law of diffusion. After a series of assumptions and simplifications, for sufficiently small current where  $\Delta E_s$  for a single titration is small, the equation for  $D_{Li}$  has been written as<sup>29</sup>

$$D_{Li} = \frac{4}{\pi} \left( \frac{m_B V_m}{M_B A} \right)^2 \left( \frac{\Delta E_s}{\tau (dE_\tau/d\sqrt{\tau})} \right)^2 \quad (\tau \ll L^2/D_{Li}) \quad [3]$$

where  $V_m$  is the molar volume of the compound,  $M_B$  and  $m_B$  are the molecular weight and mass of the host oxide, respectively,  $A$  is the total contact area between the electrolyte and the electrode, and  $L$  is the thickness of the electrode. If  $E$  vs.  $\sqrt{\tau}$  shows a straight line behavior over the entire time period of current flux, Eq. 3 can be further simplified as<sup>29</sup>

$$D_{Li} = \frac{4}{\pi \tau} \left( \frac{m_B V_m}{M_B A} \right)^2 \left( \frac{\Delta E_s}{\Delta E_\tau} \right)^2 \quad [4]$$

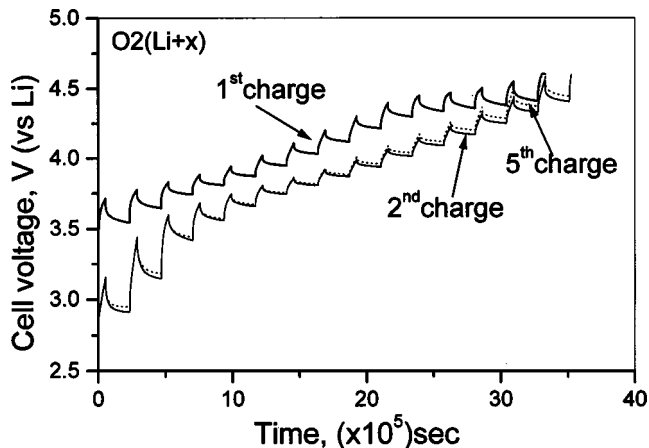
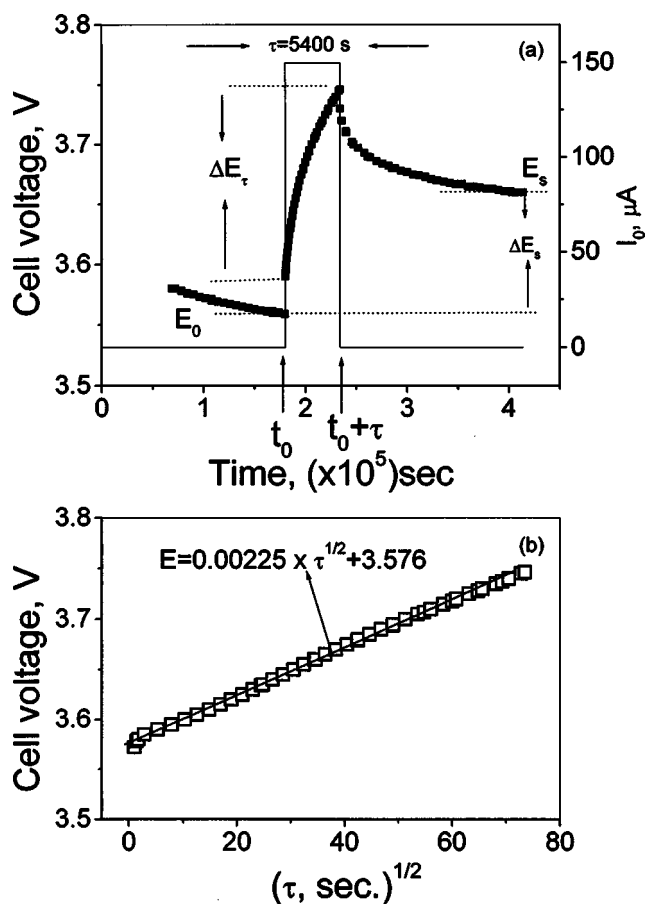


Figure 13. GITT profile for the first, second, and fifth charge cycles for the compound O2 (Li + x).

GITT measurements have been performed on O2 (Li + x) and O2 (Li) compounds to determine the  $D_{Li}$  as a function of voltage (or lithium content  $x$ ) for the entire voltage range of charge/discharge cycling (2.5–4.6 V). Figure 13 shows the GITT curves for the first, second, and fifth charge cycles for the cell with O2 (Li + x) as a function of time in the voltage window 2.5–4.6 V. The cell was charged with a constant current flux of  $I_0 = 150 \mu\text{A}$  ( $\sim C/25$  rate) for an interval of 1.5 h followed by an open circuit stand for 5 h to allow the cell voltage to relax to its steady-state value  $E_s$ . The procedure was repeated for the full voltage window of operation of the cell, 2.8–4.6 V. It is seen that the nature of the variation of equilibrium potential ( $E_s$ ) for the first charge is distinctly different from the subsequent ones. But the profile is almost identical for all the subsequent cycles (first, second, and fifth charge curves shown in Fig. 13). The applied current flux and the resulting voltage profile for a single titration at  $x = 0.76$  (corresponds to 3.66 V) during the second charge cycle of O2 (Li + x) is shown in Fig. 14 with schematic labeling of different parameters. The variation of cell voltage during the time period  $\tau$  on application of  $I_0$  at time  $t_0$ , where the cell voltage is stabilized for the above titration is plotted against  $\sqrt{\tau}$  which fits into a straight line as shown in Fig. 14b. The values of  $D_{Li}$  calculated by substituting the value of slope from Fig. 14b in Eq. 3 and that calculated using Eq. 4 from the titration curve shown in Fig. 14a at 3.66 V are  $3.1$  and  $3.2 \times 10^{-10} \text{ cm}^2/\text{s}$ , respectively. These are in close agreement and thus validate the use of Eq. 4 for the calculation of  $D_{Li}$  and the assumptions made in the derivation of Eq. 3 and 4. However, these calculations are based on the assumption that the molar volume ( $V_m$ ) remains stable with change in Li content in the compound and the possible change in it is ignored. Further, the surface area in contact with the electrolyte is taken as the geometric surface area of the electrode. It must be mentioned that the actual surface area in contact with the active material in a composite electrode system must be larger than the geometric surface area due to the penetration of electrolyte and accordingly the  $D_{Li}$  value can vary. Care has been taken to minimize this effect by making the composite electrode as thin as possible (20–25  $\mu\text{m}$ ) for the present studies. It must be also mentioned that these materials undergo a phase transition (T2 to O2) during its first Li deintercalation cycle and thereafter remain as a single phase. Therefore, diffusion can occur through the phase boundary and through each phase and the measured diffusion coefficient would be the resultant value, at least for the first charging cycle of the cell. Taking these aspects into consideration, the diffusion coefficient obtained by Eq. 3 and 4 for both compounds can be treated as the apparent rather than the true values.

The  $D_{Li}$  in the compounds O2 (Li + x) and O2 (Li) as a func-



**Figure 14.** (a) Applied current pulse vs. voltage profile for a single titration at 3.66 V ( $x = 0.76$ ) during second charge for  $O_2(Li+x)$  with schematic representation of different profile parameters. (b) Variation of cell voltage for the above titration plotted against  $\sqrt{\tau}$  to show the linear fit.

tion of cell voltage derived as above, for the first, second, fifth, and sixth charge titration cycles (similar to those shown in Fig. 13) are shown in Fig. 15. The  $V_m$  values deduced from the crystallographic data are 21.45 and 21.64  $\text{cm}^3/\text{mol}$ , respectively, for the  $O_2(Li+x)$  and  $O_2(Li)$ . The  $D_{Li}$  for the compound  $O_2(Li+x)$  shows a value of  $3.3 \times 10^{-11} \text{ cm}^2/\text{s}$  at the beginning of first charge (deintercalation) (3.54 V vs. Li) and increases by an order of magnitude at 3.64 V and reaches a maximum of  $4.2 \times 10^{-10} \text{ cm}^2/\text{s}$  at 3.74 V (Fig. 15a). The value decreases slightly and remains constant up to 4.3 V and then passes through a minimum of  $2.4 \times 10^{-11} \text{ cm}^2/\text{s}$  at 4.38 V before increasing further to a value of  $9.8 \times 10^{-11} \text{ cm}^2/\text{s}$  at the end of deintercalation. The voltage at which  $D_{Li}$  goes through a minimum coincides very well with the irreversible voltage peak observed in the CV and is due to the irreversible phase change occurring as the first deintercalation proceeds. For the second and subsequent charging titrations (up to sixth cycle shown in Fig. 15), the  $D_{Li}$  values are comparatively high and are stable in the entire voltage range, 2.75-4.6 (corresponding to the composition range  $x = 0.9-0.33$ ) with a value of  $1-3 \times 10^{-10} \text{ cm}^2/\text{s}$ . This shows that the mobility of Li ions remains almost unchanged in the  $O_2(Li+x)$  compound for the full voltage range after the initial activation and phase transition.

For the  $O_2(Li)$  compound, during the first charge cycle, the initial  $D_{Li}$  value is  $1.7 \times 10^{-10} \text{ cm}^2/\text{s}$  (3.82 V vs. Li) which decreases on delithiation to give a minimum of  $1.3 \times 10^{-11} \text{ cm}^2/\text{s}$  at 3.89 V. On further deintercalation, the  $D_{Li}$  value increases and then decreases slightly at the end of deintercalation ( $\sim 4.3$  V; Fig.

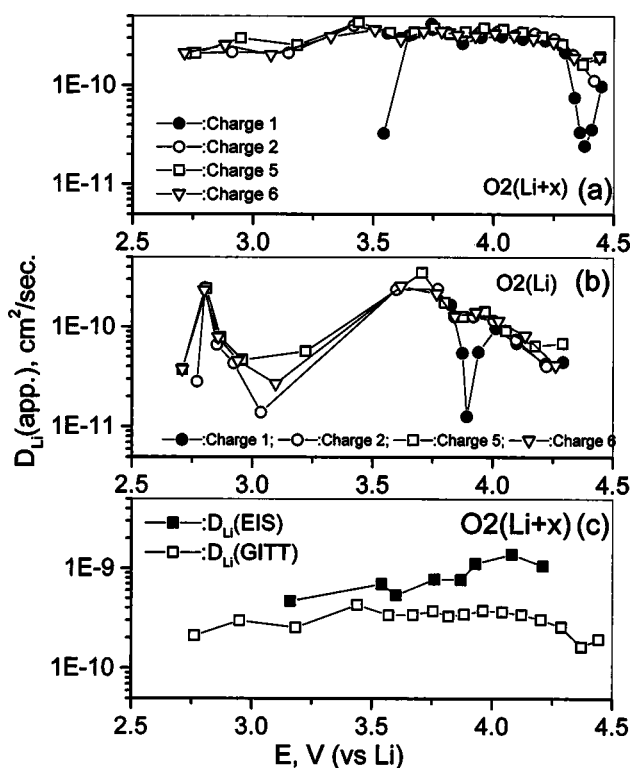


**Figure 15.**  $D_{Li}$  as a function of cell voltage obtained from different charging cycles from GITT (a) for  $O_2(Li+x)$  and (b) for  $O_2(Li)$ . (c) A comparison of  $D_{Li}$  obtained for  $O_2(Li+x)$  from EIS and GITT for the fifth charge cycle. The  $D_{Li}(\text{GITT})$  is replotted from (a).

15b). The minimum in  $D_{Li}$  during the first charge coincides with the observed CV maxima during the first anodic scan, and with the flat plateau observed in the voltage profile during the first charge, which is assigned to the T2 to  $O_2$  structural transition and/or removal of stacking faults. For the second and subsequent charge cycles, the  $D_{Li}$  values show two maxima at 2.8 and 3.7 V. Deintercalation beyond 3.7 V shows a gradual decrease in  $D_{Li}$  values until the end of charging (4.3 V). Note that the  $D_{Li}$  values show the maxima at both CV peak positions where the current through the cell is maximum (Fig. 3 and 15b). In addition to the presence of an active redox couple, the enhanced current through the cell also implies an easy migration of ions through the compound, which in fact is reflected in higher values of  $D_{Li}$  observed at these compositions (2.8 and 3.7 V). The  $D_{Li}$  values obtained in the present study are in the range observed for other layered intercalation compounds like  $\text{Li}_x\text{CoO}_2$  ( $10^{-8}$  to  $10^{-11} \text{ cm}^2/\text{s}$ ;  $x = 0.4-1.0$ ),<sup>30,32,37</sup>  $\text{Li}_x\text{NiO}_2$  ( $10^{-8}$  to  $10^{-10} \text{ cm}^2/\text{s}$ ;  $x = 0.3-0.8$ ),<sup>31,32</sup>  $\text{Li}_x\text{NiO}_2$  ( $10^{-11}$  to  $10^{-12} \text{ cm}^2/\text{s}$ ;  $V = 3.65-4.05$ ),<sup>36</sup>  $\text{Li}_x\text{Ni}_y\text{Co}_{1-y}\text{O}_2$  ( $10^{-8}$  to  $10^{-9} \text{ cm}^2/\text{s}$ ;  $x = 0.3-0.8$ ),<sup>31</sup>  $\sim 10^{-12} \text{ cm}^2/\text{s}$  ( $V = 3.7-4.2$ ),<sup>31,34</sup> and  $\sim 10^{-12} \text{ cm}^2/\text{s}$  ( $V = 3.8-4.05$ ).<sup>36</sup>

We have also determined the  $D_{Li}$  of the  $O_2(Li+x)$  compound from the impedance data by analyzing the low frequency Warburg contribution and comparing it with that obtained from the GITT data. The expression for  $D_{Li}$  from the impedance response can be written as<sup>10,23-25</sup>

$$D_{Li} = 1/2 \left[ \left( \frac{V_m}{FAA_W} \right) \frac{dE}{dx} \right]^2 \quad [5]$$

where  $V_m$  is the molar volume,  $F$  is the Faraday constant, and  $A_W$  is the Warburg coefficient which was obtained from the Warburg region of the impedance response. The  $dE/dx$  was determined from

the galvanostatic titration curve. The  $D_{\text{Li}}$  (EIS) values were deduced from the impedance data shown in Fig. 4a (fifth charge cycle) for the voltage range 3.16–4.21 V ( $x = 0.4$ –0.85) where the Warburg contribution was prominent. The  $A_{\text{W}}$  values were determined at different voltages as the average value of the slope of  $Z'$  vs.  $\omega^{-1/2}$  and  $-Z''$  vs.  $\omega^{-1/2}$  plots ( $\omega$  is the angular frequency) for the Warburg region.<sup>10,25</sup> Typical values of  $A_{\text{W}}$  at 3.54 and 3.93 V are, respectively, 8.78 and 4.16  $\Omega \text{ s}^{-1/2}$ . The  $D_{\text{Li}}$  (EIS) values thus obtained are plotted together with the values obtained for the fifth charge cycle by GITT in Fig 15c. Note that the  $D_{\text{Li}}$  (EIS) values for O2 (Li + x) are larger than those obtained by GITT by a factor of 2–4. Similar differences in  $D_{\text{Li}}$  measured for the same compound by different techniques was also reported in the literature: The  $D_{\text{Li}}$  for  $\text{Li}_x\text{CoO}_2$  in the composition range  $0.2 < x < 0.8$  obtained by GITT was  $\sim 5 \times 10^{-9} \text{ cm}^2/\text{s}$ <sup>34</sup> whereas by the EIS method, the  $D_{\text{Li}}$  values are higher by one order of magnitude.<sup>11</sup> Similarly the  $D_{\text{Li}}$  value obtained in  $\text{WO}_3$  film by EIS is one order higher than that observed by GITT.<sup>33</sup>

The variation of  $D_{\text{Li}}$  with the applied voltage, V [composition ( $x$ )] for the first charge cycle is distinctly different from the subsequent ones for both the compounds, O2 (Li + x) and O2 (Li). These compounds are known to undergo a phase transition from T2 to O2 phase structure during the first electrochemical charge which is brought about by a minor sliding in the  $\text{MO}_2$  layers.<sup>1–4,8,9</sup> This phase transition is visualized as a shift in the CV peak during first anodic scan by 0.25 V for the subsequent cycles and/or as an irreversible peak. Since the minimum in  $D_{\text{Li}}$  values as a function of voltage in the first charge cycle are coinciding with the voltage range of the irreversible peak noted in the CV of O2 (Li + x) and shifts in anodic peaks for both the compounds, this behavior is clearly associated with the initial irreversible phase change occurring in the compounds during its first deintercalation cycle. Further, the observed minimum in  $D_{\text{Li}}$  with voltage is not seen in the subsequent cycles and thus confirms the present argument. Similar minima in  $D_{\text{Li}}$  vs. voltage (or  $x$ ) plots which coincide with the CV peak positions, and are characteristic of the phase transitions were reported for other cathodes. In  $\text{Li}_x\text{CoO}_2$ , the  $D_{\text{Li}}$  vs. voltage curve shows a minimum corresponding to the 3.9 V CV peak, which is characteristic of its transition between two hexagonal phases.<sup>12,37</sup> In the spinel cathode  $\text{LiMn}_2\text{O}_4$ , the minimum in  $D_{\text{Li}}$  vs. voltage curve coincides with the CV peak characteristic of transition between two cubic phases.<sup>12</sup> Further, it is worth mentioning that the impedance response of the cells with O2 (Li + x) and O2 (Li) measured during their first charge cycle do not show any significant changes in values or shapes associated with the irreversible phase change whereas the latter is reflected in GITT and CV measurements.

The initial value of  $D_{\text{Li}}$  for the compound O2 (Li + x) ( $3.3 \times 10^{-11} \text{ cm}^2/\text{s}$  at 3.54 V) during the first charge is much lower than that for O2 (Li) ( $1.7 \times 10^{-10} \text{ cm}^2/\text{s}$  at 3.82 V) (Fig. 15a and b). This is expected since 1/3 Li sites are vacant in O2 (Li) whereas these sites are filled by the lithiation process in O2 (Li + x). The differences in the variation of  $D_{\text{Li}}$  with the full voltage range clearly demonstrate that the extra lithium incorporated into the O2 (Li + x) brings a change in its Li intercalation/deintercalation kinetics as compared to O2 (Li).

The steady state open circuit potential ( $E_{\text{ocv}}$ ) of the cells after each GITT titration was monitored and plotted vs. composition ( $x$ ) in Fig. 16 for both O2 (Li + x) and O2 (Li). As can be seen, the profiles are similar to the voltage vs. capacity profile of the cells shown in Fig. 2. The difference in voltage observed for the first and subsequent charge cycles for the O2 (Li + x) is clearly reflected in the  $E_{\text{ocv}}$  vs.  $x$  profile. Further, the clearly separated two-step processes (at 4 and 2.8 V) observed in the charge/discharge curves for the O2 (Li) in Fig. 2 are also seen in Fig. 16.

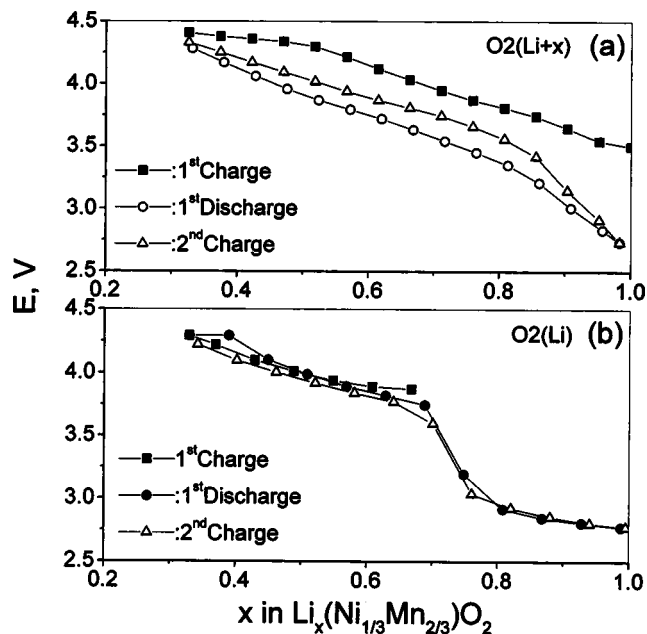


**Figure 16.** The steady-state open circuit potential ( $E_{\text{ocv}}$ ) for the first charge, first discharge, and second charge cycles as a function of lithium content  $x$  (a) for O2 (Li + x) and (b) for O2 (Li).

## Conclusions

Li-ion intercalation kinetics in the O2-structure layered manganese oxides,  $\text{Li}_{2/3}(\text{Ni}_{1/3}\text{Mn}_{2/3})\text{O}_2$  [O2 (Li)] and  $\text{Li}_{(2/3)+x}(\text{Ni}_{1/3}\text{Mn}_{2/3})\text{O}_2$  [O2 (Li + x);  $x = 1/3$ ] were elucidated by the application of EIS and GITT in conjunction with other electrochemical techniques. Modeling the EIS data with equivalent circuit approach reflects processes like Li-ion migration in the solution and through the surface film, resistance contributions from the bulk of the active material, a strongly voltage dependent charge-transfer process and solid-state Li-ion diffusion into the host materials. The formation and nature of surface film is shown to be the signature for the cell performance which in turn affects the kinetics of electrode processes. The bulk material contribution to the impedance response of the cells were detected, which varies periodically with charge/discharge cycling. The increased contribution of surface film detected on impedance response of the O2 (Li) compared to O2 (Li + x) is shown to contribute to the capacity fading observed in O2 (Li). The apparent  $D_{\text{Li}}$  for both the compounds falls in the range  $1.0 \times 10^{-11}$  to  $1.0 \times 10^{-10} \text{ cm}^2/\text{s}$  for the entire voltage range. The  $D_{\text{Li}}$  obtained from GITT and EIS are in close agreement. The irreversible phase change, from the T2 to O2 structure, observed during the first charging in these compounds is reflected as sharp minima in the  $D_{\text{Li}}$  vs. voltage in the vicinity of the irreversible peak observed in the CV of O2 (Li + x) during first oxidation cycle. The improved cycling performance of O2 (Li + x) is shown to be due to its better electrode kinetics due to the lower  $R_{\text{ct}}$  values and formation of a stable surface film.

## References

1. J. M. Paulsen, C. L. Thomas, and J. R. Dahn, *J. Electrochem. Soc.*, **147**, 861 (2000).
2. J. M. Paulsen and J. R. Dahn, *J. Electrochem. Soc.*, **147**, 2478 (2000).
3. J. M. Paulsen, R. A. Donabeger, and J. R. Dahn, *Chem. Mater.*, **12**, 2257 (2000).
4. Z. Lu and J. R. Dahn, *J. Electrochem. Soc.*, **148**, A710 (2001).
5. A. R. Armstrong, R. Gitzendanner, A. D. Robertson, and P. G. Bruce, *Chem. Commun. (Cambridge)*, **1998**, 1833.
6. Y.-M. Chiang, D. R. Sadoway, Y.-I. Jang, B. Huang, and H. Wang, *Electrochem. Solid-State Lett.*, **2**, 107 (1999).
7. K. M. Shaju, G. V. Subba Rao, and B. V. R. Chowdari, *Solid State Ionics*, In press.

8. K. M. Shaju, G. V. Subba Rao, and B. V. R. Chowdari, *Electrochem. Commun.*, **4**, 633 (2002).
9. K. M. Shaju, G. V. Subba Rao, and B. V. R. Chowdari, in *Solid State Ionics: Materials and Devices*, B. V. R. Chowdari and W. Wang, Editors, p. 225, World Scientific, Singapore (2000).
10. C. Ho, I. D. Raistrick, and R. A. Huggins, *J. Electrochem. Soc.*, **127**, 343 (1980).
11. M. G. S. R. Thomas, P. G. Bruce, and J. B. Goodenough, *J. Electrochem. Soc.*, **132**, 1521 (1985).
12. D. Aurbach, M. D. Levi, E. Levi, H. Teller, B. Markovsky, G. Salitra, U. Heider, and L. Heider, *J. Electrochem. Soc.*, **145**, 3024 (1998).
13. D. Aurbach, M. D. Levi, K. Gamolski, B. Markovsky, G. Salitra, E. Levi, U. Heider, L. Heider, and R. Oesten, *J. Power Sources*, **81-82**, 472 (1999).
14. M. D. Levi, K. Gamolski, D. Aurbach, U. Heider, and R. Oesten, *Electrochim. Acta*, **45**, 1781 (2000).
15. M. D. Levi, G. Salitra, B. Markovsky, H. Teller, D. Aurbach, U. Heider, and L. Heider, *J. Electrochem. Soc.*, **146**, 1279 (1999).
16. F. Nobili, F. Croce, B. Scrosati, and R. Marassi, *Chem. Mater.*, **13**, 1642 (2001).
17. F. Croce, F. Nobili, A. Deptula, W. Lada, R. Tossici, A. D. Epifanio, B. Scrosati, and R. Marassi, *Electrochem. Commun.*, **1**, 605 (1999).
18. F. Orsini, M. Dolle, and J.-M. Tarascon, *Solid State Ionics*, **135**, 213 (2000).
19. F. Orsini, A. D. Pasquier, B. Beaudoin, J.-M. Tarascon, M. Trentin, N. Langenhui-zen, E. D. Beer, and P. Notten, *J. Power Sources*, **76**, 19 (1998).
20. F. Nobili, R. Tossici, F. Croce, B. Scrosati, and M. Marassi, *J. Power Sources*, **94**, 238 (2001).
21. J. Fan and P. S. Fedkiw, *J. Power Sources*, **72**, 165 (1998).
22. M. Mohamedi, D. Takahashi, T. Uchiyama, T. Itoh, M. Nishizawa, and I. Uchida, *J. Power Sources*, **93**, 93 (2001).
23. D. Zhang, B. N. Popov, and R. E. White, *J. Power Sources*, **76**, 81 (1998).
24. O. Yamada, M. Ishikawa, and M. Morita, *Electrochim. Acta*, **44**, 1607 (1999).
25. S.-I. Pyun and J.-S. Bae, *Electrochim. Acta*, **41**, 919 (1996).
26. S. Zhang, M. S. Ding, K. Xu, J. Allen, and T. R. Jow, *Electrochem. Solid-State Lett.*, **4**, A206 (2001).
27. D. Aurbach, B. Markovsky, A. Schechter, Y. Ein-Eli, and H. Cohen, *J. Electrochem. Soc.*, **143**, 3809 (1996).
28. K. Dokko, M. Mohamedi, Y. Fujita, T. Itoh, M. Nishizawa, M. Umeda, and I. Uchida, *J. Electrochem. Soc.*, **148**, A422 (2001).
29. W. Weppner and R. A. Huggins, *J. Electrochem. Soc.*, **124**, 1569 (1977).
30. J.-S. Hong and J. R. Selman, *J. Electrochem. Soc.*, **147**, 3190 (2000).
31. J. Cho, H. S. Jung, Y. C. Park, G. B. Kim, and H. S. Lim, *J. Electrochem. Soc.*, **147**, 15 (2000).
32. Y.-M. Choi, S.-I. Pyun, J.-S. Bae, and S.-I. Moon, *J. Power Sources*, **56**, 25 (1995).
33. M. S. Mattsson, *Solid State Ionics*, **131**, 261 (2000).
34. M. Mizushima, P. C. Jones, P. J. Wiseman, and J. B. Goodenough, *Solid State Ionics*, **3/4**, 171 (1981).
35. C. J. Wen, B. A. Boukamp, R. A. Huggins, and W. Weppner, *J. Electrochem. Soc.*, **126**, 2258 (1979).
36. M. D. Levi, K. Gamolski, D. Aurbach, U. Heider, and R. Oesten, *J. Electroanal. Chem.*, **477**, 32 (1999).
37. Y.-I. Jang, B. J. Neudecker, and N. J. Dudney, *Electrochem. Solid-State Lett.*, **4**, A74 (2001).
38. J. M. Paulsen and J. R. Dahn, *Solid State Ionics*, **126**, 3 (1999).
39. S. Madhavi, G. V. Subba Rao, B. V. R. Chowdari, and S. F. Y. Li, *J. Power Sources*, **93**, 156 (2001).
40. C. Pouillier, L. Croguennec, Ph. Biensan, P. Willmann, and C. Delmas, *J. Electrochem. Soc.*, **147**, 2061 (2000).
41. J. M. Paulsen, C. L. Thomas, and J. R. Dahn, *J. Electrochem. Soc.*, **146**, 3560 (1999).
42. A. Kajiyama, K. Takada, T. Inada, M. Kouguchi, S. Kondo, and M. Watanabe, *J. Electrochem. Soc.*, **148**, A981 (2001).
43. Z. Lu, D. D. MacNeil, and J. R. Dahn, *Electrochem. Solid-State Lett.*, **4**, A200 (2001).
44. T. Ohzuku and Y. Makimura, *Chem. Lett.*, 642 (2001).
45. Z. Lu, D. D. MacNeil, and J. R. Dahn, *Electrochem. Solid-State Lett.*, **4**, A191 (2001).
46. T. Ohzuku and Y. Makimura, *Chem. Lett.*, 744 (2001).
47. J. Reed and G. Ceder, *Electrochem. Solid-State Lett.*, **5**, A145 (2002).
48. D. Aurbach, *J. Power Sources*, **89**, 206 (2000).
49. A. Van der Ven, M. K. Aydinol, G. Ceder, G. Kresse, and J. Hafner, *Phys. Rev. B*, **58**, 2975 (1998).
50. M. Menetrier, I. Saadoun, S. Levasseur, and C. Delmas, *J. Mater. Chem.*, **9**, 1135 (1999).
51. J. Molenda, A. Stopklosa, and T. Bak, *Solid State Ionics*, **36**, 53 (1989).
52. I. Saadoun and C. Delmas, *J. Solid State Chem.*, **136**, 8 (1998).
53. D. Carlier, M. Menetrier, and C. Delmas, *J. Mater. Chem.*, **11**, 594 (2001).
54. I. Saadoun, M. Menetrier, and C. Delmas, *J. Mater. Chem.*, **7**, 2505 (1997).